Available online at www.sciencedirect.com

ScienceDirect

International Journal of Solids and Structures 44 (2007) 7110–7142

INTERNATIONAL JOURNAL OF SOLIDS AND STRUCTURES

www.elsevier.com/locate/ijsolstr

Theoretical transient analysis and wave propagation of piezoelectric bi-materials

Chien-Ching Ma [a,*], Xi-Hong Chen [a], Yi-Shyong Ing [b]

[a] Department of Mechanical Engineering, National Taiwan University, Taipei 106, Taiwan, ROC
[b] Department of Aerospace Engineering, Tamkang University, Tamsui 251, Taiwan, ROC

Received 12 September 2006; received in revised form 5 March 2007
Available online 4 April 2007

Abstract

The transient response of piezoelectric bi-materials subjected to a dynamic anti-plane concentrated force or electric charge with perfectly bonded interface is examined in the present study. The problem is solved by using the Laplace transform method and the inverse Laplace transform is evaluated by means of Cagniard's method. Exact transient full-field solutions of the contribution for each wave are expressed in explicit closed forms. The transient behavior of field quantities is examined in detail by numerical calculations. The existence condition of a propagating surface wave along the interface is discussed in detail. A surface wave can be guided by the interface of two semi-infinite materials in contact if one, at least, of these two materials is piezoelectric. The propagation velocity of the surface wave is explicitly expressed and is found to be less than the lower shear wave velocity of the two materials. The existence of the surface wave for piezoelectric–piezoelectric bi-materials is restricted to the situation that the shear waves of the two piezoelectric materials are very close. The possibility for the existence of the surface wave for piezoelectric–elastic bi-materials is much greater than that of the piezoelectric–piezoelectric bi-materials.

Keywords: Transient response; Dynamic loading; Piezoelectric bi-materials; Surface wave; Laplace transform method

1. Introduction

The propagation of stress waves through an unbounded material is not a difficult subject. A half-space bounded by one plane surface is the simplest model for observing elastic waves in solid. Many applications of electrodynamics begin with the model of a half-space. The classical analysis in this area was first proposed by Lamb (1904); he considered the elastic half-space subjected to point and line loads on the surface of a semi-infinite half-space. Since this early analysis of Lamb, a great many contributions have appeared, pertaining to what is commonly referred to as Lamb's problem. de Hoop (1960) and Cagnard (1962) proposed a general method to evaluate the inverse Laplace transforms, which made the solving of

* Corresponding author. Tel.: +886 2 23659996; fax: +886 2 23631755.
E-mail address: ccma@ntu.edu.tw (C.-C. Ma).

0020-7683/$ - see front matter
doi:10.1016/j.ijsolstr.2007.03.027

elastic wave propagation problem become possible. The generalized ray theory was developed since 1939 when Cagniard studied the transient waves in two homogeneous half-spaces in contact. In his monumental work, he had shown that by going through a sequence of contour deformations and changes of integration variables, one is able to find the inverse Laplace transforms of the expressions for each ray. A review of this theory was given by Pao and Gajewski (1977). Spencer (1960) used the generalized ray method to investigate the surface response of a stratified half-space to the radiation from a localized source. The method leads to an infinite series of the generalized ray integral constructed in the Laplace transform domain by assembling the source function, reflection and transmission coefficient, the receiver function, and the phase function. The method therefore obviates the necessity for solving a tedious boundary value problem. The time function associated with each ray integral is obtained by using the Cagniard method. Ma and Huang (1993) have constructed the exact transient solution of buried dynamic forces for elastic bi-material problem. Buried source problems develop considerable interests in seismology and have been studied by many investigators. All the research works mentioned above are concerned with isotropic elastic materials.

Piezoelectric materials possess the important property of linear coupling between mechanical and electrical fields, which renders them useful in many areas of modern technology. These materials have thus been widely used for a long time as electromechanical transducers, filters, sensors and actuators, to mention only a few. In recent years, they are finding new applications in non-destructive evaluation, ultrasonic medical imaging, smart structures and active control of sound and vibration. In this endeavor, composite materials, consisting of combinations of two or more different piezoelectric and non-piezoelectric material phases, have been designed to meet specific technical needs. Such composites permit the tailoring of special properties, unavailable in homogeneous phases, and therefore they are becoming increasingly important in diverse areas of modern technology. Quite recently, a new class of highly advanced composites, where the material properties vary continuously in a particular direction, has been fabricated and introduced for aerospace applications. They have been termed functionally gradient materials and they are expected to play even a more important role (Yamanouchi, 1990).

The study of wave propagation in piezoelectric materials is a rather involved problem. The situation is even more formidable when non-homogeneity has to be taken into account. It is, therefore, not surprising that only scant information regarding transient wave propagation problems has been available. As in the case of the Stoneley wave, whose mechanical displacements are in the sagittal plane, the amplitude of this wave decreases with distance away from the interface into both media (Stoneley, 1924). Bleustein (1968) and Gulayev (1969) simultaneously discovered that there exists a shear horizontal (SH) electro-acoustic surface mode in a class of transversely isotropic piezoelectric media, which is known today as the BG wave. The BG wave is a unique result in the repertoire of surface acoustic wave (SAW) theory, because it has no counterpart in purely elastic solids. As a matter of fact, since then, the BG wave theory has become one of the cornerstones for the modern electro-acoustic technology. It is shown that BG wave can exist in cubic crystals of $\bar{4}3m$ and 23 classes, along [1 1 0] direction on the $(\bar{1}10)$ plane and their equivalent orientations. The velocity equations for piezoelectric surface wave and elastic surface wave were derived and their characteristics were discussed by Tseng (1970). A pure shear elastic surface wave (MT wave) can propagate along the interface of two identical crystals, in class 6 mm, when the z-axis of these crystals, both parallel to the interface and perpendicular to the propagation direction, are in opposite directions (Maerfeld and Tournois, 1971). The general equations and the fundamental piezoelectric matrix were derived for the anti-plane wave motion and Floquet theory was applied to obtain the passing and stopping bands in a periodically layered infinite space by Honein and Herrman (1992). Taking into account both optical effect as well as the contribution from the rotational part of electric field, the solutions obtained were not only valid for any wave speed range, but also provide accurate formulas to evaluate the acousto-optic interaction due to piezoelectricity. As the wave speed is much less than the speed of light, the solution degenerates to the well-known BG wave or MT wave (Li, 1996).

The surface acoustic wave (SAW) can be excited and detected efficiently by using an interdigital transducer (IDT) placed on a piezoelectric substrate and a vast amount of effort was invested in the research and development of SAW devices for military and communication applications, such as delay lines and filters for radar. The propagation mode in most devices is the Rayleigh wave on a free surface of a piezoelectric substrate. Since SAWs concentrate their energy near the substrate free surface, their propagation surface should be sufficiently flat and free of contamination. This means that devices based on SAWs must be put into a package for protection against surface disturbance. The packages are usually much larger than the substrate and account for most of the cost of the device. Hence it is difficult to satisfy the requirement for smaller device and reliability.

With the fast evolution of passive high frequency filtering requirements, much effort has been devoted to the improvement of classical SAW. Among possible new devices, the use of interface surface waves (ISWs) in place of SAWs has been proposed. As one of the families of such ISWs, Stoneley waves, which basically consist of longitudinal and shear-vertical displacement components, have been most extensively discussed in the past. Because of the very restricted range of existence of Stoneley waves and this acoustic wave can not be excited by interdigital transducers in such nonpiezoelectric media, it has been rather difficult to find practical device applications. Hence a piezoelectric material must be chosen as one or both media. Recently, some technologies appeared that allow one to create a direct contact between two previously grown piezocrystals of different symmetry (Dvoesherstov et al., 2002). Accordingly, interest in the development of interface surface waves has grown considerably. Camou and Laude (2003) used a interdigital transducer at the interface for the excitation of the ISW. The application of interface surface waves in acousto-electronic devices can give a number of important advantages over the common SAW. One of the most cited advantages of ISW devices as opposed to SAW devices is the natural protection of the excitation interface, which is isolated from, and hence insensitive to, external disturbances, such as dust or wetness. This should lead to a simplification of packaging requirements, especially at high frequencies. Furthermore, in some cases, the phase velocity of transverse ISWs can be higher than that of SAWs. By choosing specific piezoelectric media, one can also improve the parameters of the wave, namely, raise the electromechanical coupling coefficient and improve the thermal stability of the wave simultaneously (Irino et al., 1988; Irino and Shimizu, 1989). It was pointed out by Yamashita et al. (1997) that the penetration depth of shear-horizontal type of ISWs into the bulk is small. Hence the substrate thickness needed for practical applications can be reduced to several wavelengths. This suggests that the direct wafer bonding technique could be applied to realize the structure.

A lot of engineering applications mentioned above are involved with wave propagations through the piezoelectric components, and hence their dynamic or transient behaviors are the primary concern in design as well as in performance. In this paper, an analysis is presented to study the transient behaviors of a transversely isotropic piezoelectric material under anti-plane mechanical and in-plane electrical line sources, which is considered as one of the fundamental important problems in electro-elastodynamics. This problem exhibits the distinct feature of piezoelectricity, which is different from the behaviors of ordinary elasto-dielectric solids. The analysis presented in this study provides a sound theoretical ground and interesting physics for a better understanding of the transient behaviors of piezoelectric materials. The results obtained in this study will be useful for the design and application of ISWs devices. This article is divided into five sections. Following this brief introduction, Section 2 outlines the basic equations needed to formulate the problem. The exact full-field transient solutions for piezoelectric bi-materials are presented in explicit forms. The possibility that there exists a piezoelectrically-induced electromagnetic surface wave propagating along the interface between two materials is discussed in detail in Section 3. Then, a number of numerical results of transient behaviors for interesting cases and the surface wave velocity along the interface of bi-materials are examined in Section 4. Finally we conclude the paper in Section 5.

2. The transient solutions for piezoelectric bi-materials

In a piezoelectric material, the interdependence of electric and mechanical fields implies coupling elastic and electromagnetic waves. Because elastic waves in a typical material are five orders of magnitude slower than electromagnetic waves, so the piezoelectrically coupled electric field is assumed to be quasi-static. Maxwell's equations therefore reduce to (Hayt and Buck, 2001)

$$D_{i,i} = \rho_s, \tag{1}$$

$$E_i = -\Phi_{,i} \tag{2}$$

where D_i, E_i, Φ and ρ_s are electric displacement, electric field, electrostatic potential and free charge density, respectively, and the comma denotes differentiation in the usual tensor notation. The piezoelectric material is assumed to be a perfect insulator so that ρ_s is zero, then (1) reduces to the Laplace's equation

$$\Phi_{,ii} = 0 \tag{3}$$

Consequently, the propagation of elastic and electromagnetic waves can be treated separately. The mechanical field quantities must satisfy Newton's stress equation of motion which, in absence of internal body forces, becomes

$$\tau_{ij,j} = \rho\ddot{u}_i \tag{4}$$

where τ_{ij}, u_i and ρ are stress tensor, mechanical displacement and density, respectively, and the dot denotes the differentiation with respect to time. Infinitesimal strain tensor S_{ij} is defined by

$$S_{ij} = \frac{1}{2}(u_{i,j} + u_{j,i}). \tag{5}$$

The above relationships are coupled through the piezoelectric equations of state

$$\tau_{ij} = c_{ijkl}S_{kl} - e_{kij}E_k, \tag{6}$$

$$D_i = e_{ikl}S_{kl} + \varepsilon_{ik}E_k, \tag{7}$$

where c_{ijkl}, e_{kij} and ε_{ik} are the elastic, piezoelectric and permittivity tensors of the material, respectively. Substituting (2)–(5) into (6) and (7), the second-order coupled differential equations of the system for u_l and Φ are obtained (Royer and Dieulesaint, 2000)

$$c_{ijkl}u_{l,jk} + e_{kij}\Phi_{,kj} = \rho\ddot{u}_i, \tag{8}$$

$$e_{jkl}u_{l,jk} - \varepsilon_{jk}\Phi_{,jk} = 0. \tag{9}$$

In what follows, the wave polarized in the z-direction, propagating in the x–y plane of a hexagonal crystal in class $6mm$ will be analyzed. The x, y and z axes are aligned with the crystal axes X, Y and Z, respectively. In this configuration, the boundary value problem simplifies considerably because there exists the anti-plane displacement u_z, which couples only with the in-plane electric fields E_x and E_y, such that

$$u_z = w(x, y, t), \quad E_x = E_x(x, y, t), \quad E_y = E_y(x, y, t). \tag{10}$$

This is the so-called anti-plane problem, upon substituting these relations into (8) and (9), we are led to

$$c_{44}\nabla^2 w + e_{15}\nabla^2\Phi = \rho\ddot{w}, \tag{11}$$

$$e_{15}\nabla^2 w - \varepsilon_{11}\nabla^2\Phi = 0, \tag{12}$$

where ∇^2 is the two-dimensional Laplacian operator and $\nabla^2 \equiv \frac{\partial^2}{\partial x^2} + \frac{\partial^2}{\partial y^2}$. The constitutive equations can be simplified as

$$\tau_{yz} = c_{44}\frac{\partial w}{\partial y} + e_{15}\frac{\partial \Phi}{\partial y}, \tag{13}$$

$$D_y = e_{15}\frac{\partial w}{\partial y} - \varepsilon_{11}\frac{\partial \Phi}{\partial y}, \tag{14}$$

$$\tau_{xz} = c_{44}\frac{\partial w}{\partial x} + e_{15}\frac{\partial \Phi}{\partial x}, \tag{15}$$

$$D_x = e_{15}\frac{\partial w}{\partial x} - \varepsilon_{11}\frac{\partial \Phi}{\partial x}. \tag{16}$$

We define a function ψ by

$$\psi \equiv \Phi - \frac{e_{15}}{\varepsilon_{11}} w. \tag{17}$$

The solutions of (11) and (12) can be obtained from the solutions of the following two uncoupled equations

$$\nabla^2 w = \frac{\rho}{\bar{c}_{44}} \ddot{w}, \tag{18}$$

$$\nabla^2 \psi = 0, \tag{19}$$

where $\bar{c}_{44} \equiv c_{44} + \frac{e_{15}^2}{\varepsilon_{11}}$ is the piezoelectrically stiffened elastic constant. The constitutive equations are reduced to the form of

$$\tau_{yz} = \bar{c}_{44} \frac{\partial w}{\partial y} + e_{15} \frac{\partial \psi}{\partial y}, \tag{20}$$

$$D_y = -\varepsilon_{11} \frac{\partial \psi}{\partial y}, \tag{21}$$

$$\tau_{xz} = \bar{c}_{44} \frac{\partial w}{\partial x} + e_{15} \frac{\partial \psi}{\partial x}, \tag{22}$$

$$D_x = -\varepsilon_{11} \frac{\partial \psi}{\partial x}. \tag{23}$$

2.1. The transient solutions for applying a dynamic anti-plane concentrated force

In this problem, the system of coordinates (x, y, z) is chosen so that perfectly conducting plane is described by the equation $y = 0$, as shown in Fig. 1. This is also an interface between two half-spaces of piezoelectric materials. The piezoelectric bi-material is initially undisturbed. Material (1) is subjected to a dynamic anti-plane concentrated force at $x = 0$, $y = d$ with magnitude p at time $t = 0$. The jump condition for the shear stress is

$$\tau_{yz}^{(1^+)}|_{y=d} - \tau_{yz}^{(1^-)}|_{y=d} = p\delta(x)\mathrm{H}(t), \tag{24}$$

where $\delta(x)$ is the delta function of x and $\mathrm{H}(t)$ is the Heaviside function of t. The continuous conditions are

$$D_y^{(1^+)}|_{y=d} - D_y^{(1^-)}|_{y=d} = 0, \tag{25}$$

$$w^{(1^+)}|_{y=d} - w^{(1^-)}|_{y=d} = 0, \tag{26}$$

$$\Phi^{(1^+)}|_{y=d} - \Phi^{(1^-)}|_{y=d} = 0, \tag{27}$$

$$\tau_{yz}^{(1^-)}|_{y=0} = \tau_{yz}^{(2)}|_{y=0}, \tag{28}$$

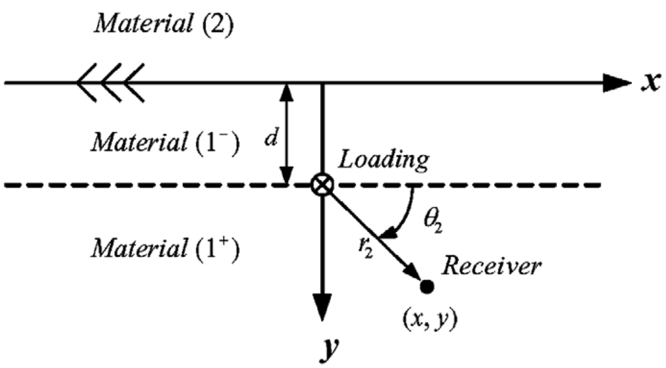

Fig. 1. The geometric configuration of a piezoelectric bi-material and the coordinate system.

$$D_y^{(1^-)}|_{y=0} = D_y^{(2)}|_{y=0}, \tag{29}$$

$$w^{(1^-)}|_{y=0} = w^{(2)}|_{y=0}, \tag{30}$$

$$\Phi^{(1^-)}|_{y=0} = \Phi^{(2)}|_{y=0}. \tag{31}$$

Note that, the superscripts (1) and (2) indicate materials (1) and (2), respectively. This problem can be solved by the application of integral transforms. The one-sided Laplace transform over time t and the bilateral Laplace transform on the spatial variable x for (18) and (19) can be represented of the form

$$\frac{d^2\bar{w}^*}{dy^2} - (b^2 - \lambda^2)s^2\bar{w}^* = 0, \tag{32}$$

$$\frac{d^2\bar{\psi}^*}{dy^2} - (\varepsilon^2 - \lambda^2)s^2\bar{\psi}^* = 0, \tag{33}$$

where s which is the Laplace transform parameter is a positive real number, large enough to ensure the convergence of the integral and λ is a complex variable. Where $b = \sqrt{\frac{\rho}{\bar{c}_{44}}}$ is the slowness of the shear wave and $\varepsilon \to 0^+$. The overbar symbol is used denoting the transform on time t and the star symbol is used denoting the transform on the spatial variable x. The general solutions of (32) and (33) represented in the matrix form are

$$\begin{bmatrix} \bar{w}^{*(1^+)} \\ \bar{\psi}^{*(1^+)} \end{bmatrix} = \mathbf{Y}^{-1}\begin{bmatrix} A_1 \\ C_1 \end{bmatrix} + \mathbf{Y}\begin{bmatrix} B_1 \\ D_1 \end{bmatrix}, \tag{34}$$

$$\begin{bmatrix} \bar{w}^{*(1^-)} \\ \bar{\psi}^{*(1^-)} \end{bmatrix} = \mathbf{Y}^{-1}\begin{bmatrix} E_1 \\ G_1 \end{bmatrix} + \mathbf{Y}\begin{bmatrix} F_1 \\ H_1 \end{bmatrix}, \tag{35}$$

$$\begin{bmatrix} \bar{w}^{*(2)} \\ \bar{\psi}^{*(2)} \end{bmatrix} = \mathbf{Y}^{*-1}\begin{bmatrix} I_1 \\ K_1 \end{bmatrix} + \mathbf{Y}^*\begin{bmatrix} J_1 \\ L_1 \end{bmatrix}, \tag{36}$$

where

$$\mathbf{Y} = \begin{bmatrix} e^{s\alpha y} & 0 \\ 0 & e^{s\beta y} \end{bmatrix}, \quad \mathbf{Y}^{-1} = \begin{bmatrix} e^{-s\alpha y} & 0 \\ 0 & e^{-s\beta y} \end{bmatrix}, \quad \mathbf{Y}^* = \begin{bmatrix} e^{s\alpha^* y} & 0 \\ 0 & e^{s\beta y} \end{bmatrix}, \quad \mathbf{Y}^{*-1} = \begin{bmatrix} e^{-s\alpha^* y} & 0 \\ 0 & e^{-s\beta y} \end{bmatrix},$$

$$\alpha(\lambda) = \sqrt{b_1^2 - \lambda^2}, \quad \beta(\lambda) = \sqrt{\varepsilon^2 - \lambda^2}, \quad \alpha^*(\lambda) = \sqrt{b_2^2 - \lambda^2}, \quad b_1 = \sqrt{\frac{\rho^{(1)}}{\bar{c}_{44}^{(1)}}}, \quad b_2 = \sqrt{\frac{\rho^{(2)}}{\bar{c}_{44}^{(2)}}}.$$

The coefficients A_1, B_1, C_1, D_1, E_1, F_1, G_1, H_1, I_1, J_1, K_1 and L_1 are determined by satisfying the jump and continuous conditions. The solutions of the mechanical and electric fields presented in the Laplace transform domain are

$$\begin{bmatrix} \bar{w}^{*(1)} \\ \bar{\psi}^{*(1)} \end{bmatrix} = \frac{-1}{2s^2}(\mathbf{Y}^{-1}\mathbf{R}\mathbf{D}^{-1}\mathbf{M}^{-1}\mathbf{Z} + \mathbf{B}\mathbf{M}^{-1}\mathbf{Z}), \tag{37}$$

$$\begin{bmatrix} \bar{w}^{*(2)} \\ \bar{\psi}^{*(2)} \end{bmatrix} = \frac{-1}{2s^2}\mathbf{Y}^*\mathbf{Q}\mathbf{T}\mathbf{D}^{-1}\mathbf{M}^{-1}\mathbf{Z}, \tag{38}$$

$$\begin{bmatrix} \bar{\tau}_{yz}^{*(1)} \\ \bar{D}_y^{*(1)} \end{bmatrix} = \frac{1}{2s}(\mathbf{M}_1\mathbf{U}\mathbf{Y}^{-1}\mathbf{R}\mathbf{D}^{-1}\mathbf{M}^{-1}\mathbf{Z} + \mathbf{M}_1\mathbf{U}\mathbf{B}\mathbf{M}^{-1}\mathbf{Z}), \tag{39}$$

$$\begin{bmatrix} \bar{\tau}_{xz}^{*(1)} \\ \bar{D}_x^{*(1)} \end{bmatrix} = \frac{-1}{2s}(\mathbf{M}_1\boldsymbol{\lambda}_\mathbf{a}\mathbf{Y}^{-1}\mathbf{R}\mathbf{D}^{-1}\mathbf{M}^{-1}\mathbf{Z} + \mathbf{M}_1\boldsymbol{\lambda}_\mathbf{b}\mathbf{B}\mathbf{M}^{-1}\mathbf{Z}), \tag{40}$$

$$\begin{bmatrix} \bar{\tau}_{yz}^{*(2)} \\ \bar{D}_{y}^{*(2)} \end{bmatrix} = \frac{-1}{2s}\mathbf{N}_1\mathbf{V}\mathbf{Y}^*\mathbf{Q}\mathbf{T}\mathbf{D}^{-1}\mathbf{M}^{-1}\mathbf{Z}, \tag{41}$$

$$\begin{bmatrix} \bar{\tau}_{xz}^{*(2)} \\ \bar{D}_{x}^{*(2)} \end{bmatrix} = \frac{-1}{2s}\mathbf{N}_1\boldsymbol{\lambda}_\mathbf{c}\mathbf{Y}^*\mathbf{Q}\mathbf{T}\mathbf{D}^{-1}\mathbf{M}^{-1}\mathbf{Z}, \tag{42}$$

where

$$\mathbf{M} = \begin{bmatrix} \bar{c}_{44}^{(1)}\alpha & e_{15}^{(1)}\beta \\ 0 & -\varepsilon_{11}^{(1)}\beta \end{bmatrix}, \quad \mathbf{N} = \begin{bmatrix} \bar{c}_{44}^{(2)}\alpha^* & e_{15}^{(2)}\beta \\ 0 & -\varepsilon_{11}^{(2)}\beta \end{bmatrix}, \quad \mathbf{M}_1 = \begin{bmatrix} \bar{c}_{44}^{(1)} & e_{15}^{(1)} \\ 0 & -\varepsilon_{11}^{(1)} \end{bmatrix}, \quad \mathbf{N}_1 = \begin{bmatrix} \bar{c}_{44}^{(2)} & e_{15}^{(2)} \\ 0 & -\varepsilon_{11}^{(2)} \end{bmatrix},$$

$$\mathbf{R} = (\mathbf{M}+\mathbf{N}\mathbf{Q})^{-1}(\mathbf{M}-\mathbf{N}\mathbf{Q}), \quad \mathbf{T} = (\mathbf{M}+\mathbf{N}\mathbf{Q})^{-1}(\mathbf{M}-\mathbf{N}\mathbf{Q})+\mathbf{I}, \quad \boldsymbol{\lambda}_\mathbf{a} = \begin{bmatrix} \lambda_1^+ & 0 \\ 0 & \lambda_3^+ \end{bmatrix},$$

$$\boldsymbol{\lambda}_\mathbf{b} = \begin{bmatrix} \lambda_2^+ & 0 \\ 0 & \lambda_4^+ \end{bmatrix}, \quad \boldsymbol{\lambda}_\mathbf{c} = \begin{bmatrix} \lambda_5^+ & 0 \\ 0 & \lambda_6^+ \end{bmatrix}, \quad \mathbf{U} = \begin{bmatrix} \alpha & 0 \\ 0 & \beta \end{bmatrix}, \quad \mathbf{V} = \begin{bmatrix} \alpha^* & 0 \\ 0 & \beta \end{bmatrix}, \quad \mathbf{D}^{-1} = \begin{bmatrix} e^{-s\alpha d} & 0 \\ 0 & e^{-s\beta d} \end{bmatrix},$$

$$\mathbf{B} = \begin{bmatrix} e^{-s\alpha|y-d|} & 0 \\ 0 & e^{-s\beta|y-d|} \end{bmatrix}, \quad \mathbf{I} = \begin{bmatrix} 1 & 0 \\ 0 & 1 \end{bmatrix}, \quad \mathbf{Q} = \begin{bmatrix} 1 & 0 \\ \frac{e_{15}^{(1)}}{\varepsilon_{11}^{(1)}} - \frac{e_{15}^{(2)}}{\varepsilon_{11}^{(2)}} & 1 \end{bmatrix}, \quad \mathbf{Z} = \begin{bmatrix} p \\ 0 \end{bmatrix}.$$

The next step consists in evaluating the inverse Laplace transform of (37)–(42) by means of the Cagniard-de Hoop scheme. The Cagniard-de Hoop inversion method is used to perform the two integrations in one single operation leaving only the convolution to be done. We have to include the integral around the branch cut whatever different slowness combines. This additional integral path represents the head wave. There are two situations, $b_1|\cos\theta_1| > b_2$ and $b_1|\cos\theta_1| < b_2$, to be investigated and the λ-contours are shown in Fig. 2. As the Cagniard-de Hoop inversion method is employed, we introduce Cagniard contours by setting

$$\alpha(y+d) - \lambda x = t, \tag{43}$$

$$\alpha(y-d) - \lambda x = t, \tag{44}$$

$$\beta y + \alpha d - \lambda x = t, \tag{45}$$

$$\beta(y-d) - \lambda x = t, \tag{46}$$

$$-\alpha^* y + \alpha d - \lambda x = t, \tag{47}$$

$$-\beta y + \alpha d - \lambda x = t. \tag{48}$$

Note that, vales of $\lambda_1^\pm$, $\lambda_2^\pm$, $\lambda_3^\pm$, $\lambda_4^\pm$, $\lambda_5^\pm$ and $\lambda_6^\pm$ are the roots of (43)–(47) and (48), respectively. When the imaginary part of root in (45) and (48) vanishes, the correspondent arrive times are denoted by t_3 and t_6, respectively. The additional integral path represents the head wave in (43) and (47), where the wave fronts of head wave arrive at time $t = t_{1HD}$ and $t = t_{5HD}$, respectively.

Finally, the transient solutions in matrix form for displacement, shear stresses and electric displacement for piezoelectric materials (1) and (2) are explicitly presented and are summarized as follows

$$\begin{bmatrix} w^{(1)} \\ \psi^{(1)} \end{bmatrix} = \frac{-1}{2\pi}\left(\int_0^t \mathbf{H}_\mathbf{a}\mathrm{Im}[\boldsymbol{\lambda}'_\mathbf{a}\mathbf{R}\mathbf{M}^{-1}\mathbf{Z}]\,\mathrm{d}t + \int_0^t \mathbf{H}_\mathbf{b}\mathrm{Im}[\boldsymbol{\lambda}'_\mathbf{b}\mathbf{M}^{-1}\mathbf{Z}]\,\mathrm{d}t\right), \tag{49}$$

$$\begin{bmatrix} w^{(2)} \\ \psi^{(2)} \end{bmatrix} = \frac{-1}{2\pi}\int_0^t \mathbf{H}_\mathbf{c}\mathrm{Im}[\boldsymbol{\lambda}'_\mathbf{c}\mathbf{Q}\mathbf{T}\mathbf{M}^{-1}\mathbf{Z}]\,\mathrm{d}t, \tag{50}$$

$$\begin{bmatrix} \tau_{yz}^{(1)} \\ D_{y}^{(1)} \end{bmatrix} = \frac{1}{2\pi}(\mathrm{Im}[\mathbf{H}_\mathbf{a}\boldsymbol{\lambda}'_\mathbf{a}\mathbf{M}_1\mathbf{U}\mathbf{R}\mathbf{M}^{-1}\mathbf{Z}] + \mathrm{Im}[\mathbf{H}_\mathbf{b}\boldsymbol{\lambda}'_\mathbf{b}\mathbf{M}_1\mathbf{U}\mathbf{M}^{-1}\mathbf{Z}]), \tag{51}$$

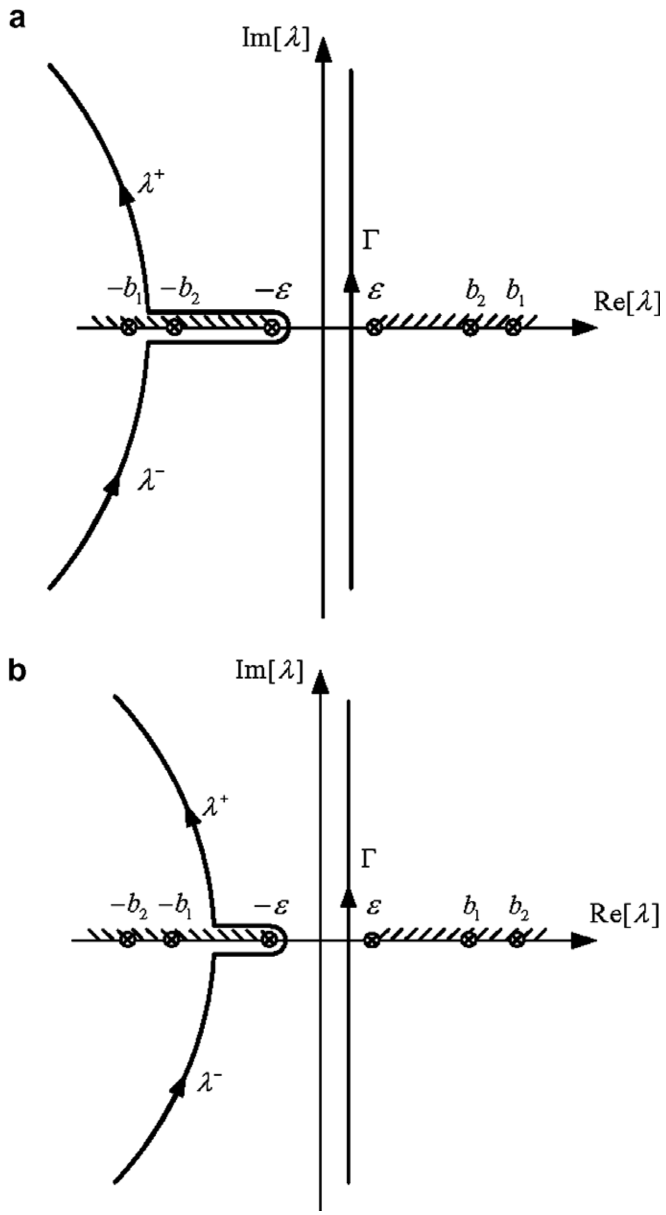

Fig. 2. The Cagniard-de Hoop contour for (a) $b_1|\cos\theta_1| > b_2$ and (b) $b_1|\cos\theta_1| < b_2$.

$$\begin{bmatrix} \tau_{xz}^{(1)} \\ D_x^{(1)} \end{bmatrix} = \frac{-1}{2\pi}\left(\mathrm{Im}[\mathbf{H_a}\boldsymbol{\lambda}'_{\mathbf{a}}\mathbf{M}_1\boldsymbol{\lambda}_{\mathbf{a}}\mathbf{R}\mathbf{M}^{-1}\mathbf{Z}] + \mathrm{Im}[\mathbf{H_b}\boldsymbol{\lambda}'_{\mathbf{b}}\mathbf{M}_1\boldsymbol{\lambda}_{\mathbf{b}}\mathbf{M}^{-1}\mathbf{Z}]\right), \tag{52}$$

$$\begin{bmatrix} \tau_{yz}^{(2)} \\ D_y^{(2)} \end{bmatrix} = \frac{-1}{2\pi}\mathrm{Im}[\mathbf{H_c}\boldsymbol{\lambda}'_{\mathbf{c}}\mathbf{N}_1\mathbf{VQTM}^{-1}\mathbf{Z}], \tag{53}$$

$$\begin{bmatrix} \tau_{xz}^{(2)} \\ D_x^{(2)} \end{bmatrix} = \frac{-1}{2\pi}\mathrm{Im}[\mathbf{H_c}\boldsymbol{\lambda}'_{\mathbf{c}}\mathbf{N}_1\boldsymbol{\lambda}_{\mathbf{c}}\mathbf{QTM}^{-1}\mathbf{Z}], \tag{54}$$

where

$$\boldsymbol{\lambda}'_{\mathbf{a}} = \begin{bmatrix} \frac{\partial\lambda_1^+}{\partial t} & 0 \\ 0 & \frac{\partial\lambda_3^+}{\partial t} \end{bmatrix}, \quad \boldsymbol{\lambda}'_{\mathbf{b}} = \begin{bmatrix} \frac{\partial\lambda_2^+}{\partial t} & 0 \\ 0 & \frac{\partial\lambda_4^+}{\partial t} \end{bmatrix}, \quad \boldsymbol{\lambda}'_{\mathbf{c}} = \begin{bmatrix} \frac{\partial\lambda_5^+}{\partial t} & 0 \\ 0 & \frac{\partial\lambda_6^+}{\partial t} \end{bmatrix}, \quad \mathbf{H_a} = \begin{bmatrix} \mathrm{H}(t-t_{1HD}) & 0 \\ 0 & \mathrm{H}(t-t_3) \end{bmatrix}$$

$$\mathbf{H_b} = \begin{bmatrix} \mathrm{H}(t-b_1 r_2) & 0 \\ 0 & \mathrm{H}(t-\varepsilon r_2) \end{bmatrix}, \quad \mathbf{H_c} = \begin{bmatrix} \mathrm{H}(t-t_{5HD}) & 0 \\ 0 & \mathrm{H}(t-t_6) \end{bmatrix}, \quad r_1 = \sqrt{x^2+(y+d)^2}, \; r_2 = \sqrt{x^2+(y-d)^2},$$

$$\lambda_1^+ = -\frac{t}{r_1}\cos\theta_1 + \mathrm{i}|\sin\theta_1|\sqrt{\frac{t^2}{r_1^2} - b_1^2}, \quad \lambda_2^+ = -\frac{t}{r_2}\cos\theta_2 + \mathrm{i}|\sin\theta_2|\sqrt{\frac{t^2}{r_2^2} - b_1^2}, \quad t_{1HD} = b_1(r_2\sin\theta_2 + d),$$

$$t_{5HD} = -b_2(r_2\sin\theta_2 + d) + b_1 d, \quad \cos\theta_1 = \frac{x}{r_1}, \quad \sin\theta_1 = \frac{(y+d)}{r_1}, \quad \cos\theta_2 = \frac{x}{r_2}, \quad \sin\theta_2 = \frac{(y-d)}{r_2}.$$

The transient solutions in matrix form presented in (51)–(54) can also be completely expressed in explicit form as indicated in Appendix A. If the piezoelectric material (2) is reduced to an elastic material, which implies that the piezoelectric effect is neglected. Then we have

$$\bar{c}_{44}^{(2)} = \mu, \tag{55}$$

$$e_{15}^{(2)} = 0, \tag{56}$$

$$\varepsilon_{11}^{(2)} \to \infty, \tag{57}$$

where μ is shear modulus. Substitution of (55)–(57) into (49)–(54) yields the transient solutions in matrix form for displacement, stress and electric displacement for piezoelectric and elastic bi-material.

2.2. The transient solutions for applying a dynamic electric charge

In this problem, the material (1) is subjected to a dynamic electric charge ($-q\delta(x)\mathrm{H}(t)$) at time $t = 0$, as shown in Fig. 1. The jump condition is represented as

$$D_y^{(1^+)}|_{y=d} - D_y^{(1^-)}|_{y=d} = -q\delta(x)\mathrm{H}(t). \tag{58}$$

The continuous conditions are the same as that presented in (26)–(31) and the jump of shear stress τ_{yz} in (24) equal zero. The Cagniard-de Hoop inversion method is applied and Cagniard contours are introduced by setting (43)–(48) and

$$\alpha y + \beta d - \lambda x = t, \tag{59}$$

$$\beta(y+d) - \lambda x = t, \tag{60}$$

$$-\alpha^* y + \beta d - \lambda x = t, \tag{61}$$

$$-\beta(y-d) - \lambda x = t. \tag{62}$$

Note that vales of $\lambda_7^\pm$, $\lambda_8^\pm$, $\lambda_9^\pm$ and $\lambda_{10}^\pm$ are the roots of (59)–(62), respectively. When the imaginary part of root in (59) and (61) vanishes, the correspondent arrive times are denoted by t_7 and t_9, respectively. Accordingly, from the similar procedure that we have used for applying a dynamic concentrated force, the transient solutions for displacement, shear stresses and electric displacements for piezoelectric materials (1) and (2) are summarized as follows

$$\begin{bmatrix} w^{(1)} \\ \psi^{(1)} \end{bmatrix} = \frac{-1}{2\pi}\left(\int_0^t \mathbf{H_a}\mathrm{Im}[\boldsymbol{\lambda}'_{\mathbf{a}}\mathbf{R}\mathbf{M}^{-1}\mathbf{G}]\,\mathrm{d}t + \int_0^t \mathbf{H_b}\mathrm{Im}[\boldsymbol{\lambda}'_{\mathbf{b}}\mathbf{M}^{-1}\mathbf{G}]\,\mathrm{d}t\right), \tag{63}$$

$$\begin{bmatrix} w^{(2)} \\ \psi^{(2)} \end{bmatrix} = \frac{-1}{2\pi}\int_0^t \mathbf{H_c}\mathrm{Im}[\boldsymbol{\lambda}'_{\mathbf{c}}\mathbf{Q}\mathbf{T}\mathbf{M}^{-1}\mathbf{G}]\,\mathrm{d}t, \tag{64}$$

$$\begin{bmatrix} \tau_{yz}^{(1)} \\ D_y^{(1)} \end{bmatrix} = \frac{1}{2\pi}(\mathrm{Im}[\mathbf{M}_1\mathbf{U}\mathbf{H_d}\mathbf{R}\boldsymbol{\lambda}'_{\mathbf{d}}\mathbf{M}^{-1}\mathbf{G}] + \mathrm{Im}[\mathbf{M}_1\mathbf{U}\mathbf{H_e}\boldsymbol{\lambda}'_{\mathbf{e}}\mathbf{M}^{-1}\mathbf{G}]), \tag{65}$$

$$\begin{bmatrix} \tau_{xz}^{(1)} \\ D_x^{(1)} \end{bmatrix} = \frac{-1}{2\pi}(\mathrm{Im}[\mathbf{M}_1\boldsymbol{\lambda}_{\mathbf{d}}\mathbf{H_d}\mathbf{R}\boldsymbol{\lambda}'_{\mathbf{d}}\mathbf{M}^{-1}\mathbf{G}] + \mathrm{Im}[\mathbf{M}_1\boldsymbol{\lambda}_{\mathbf{e}}\mathbf{H_e}\boldsymbol{\lambda}'_{\mathbf{e}}\mathbf{M}^{-1}\mathbf{G}]), \tag{66}$$

$$\begin{bmatrix} \tau_{yz}^{(2)} \\ D_y^{(2)} \end{bmatrix} = \frac{-1}{2\pi}\mathrm{Im}[\mathbf{N}_1\mathbf{V}\mathbf{H_f}\mathbf{Q}\mathbf{T}\boldsymbol{\lambda}'_{\mathbf{f}}\mathbf{M}^{-1}\mathbf{G}], \tag{67}$$

$$\begin{bmatrix} \tau_{xz}^{(2)} \\ D_x^{(2)} \end{bmatrix} = \frac{-1}{2\pi}\mathrm{Im}[\mathbf{N}_1\boldsymbol{\lambda}_{\mathbf{f}}\mathbf{H_f}\mathbf{Q}\mathbf{T}\boldsymbol{\lambda}'\mathbf{M}^{-1}\mathbf{G}], \tag{68}$$

where

$$\mathbf{G} = \begin{bmatrix} 0 \\ -q \end{bmatrix}, \quad \boldsymbol{\lambda}'_{\mathbf{d}} = \begin{bmatrix} \lambda'_{d1} & 0 \\ 0 & \lambda'_{d3} \end{bmatrix}, \quad \boldsymbol{\lambda}'_{\mathbf{e}} = \begin{bmatrix} \lambda'_{e2} & 0 \\ 0 & \lambda'_{e4} \end{bmatrix}, \quad \boldsymbol{\lambda}'_{\mathbf{f}} = \begin{bmatrix} \lambda'_{f5} & 0 \\ 0 & \lambda'_{f6} \end{bmatrix}, \quad \boldsymbol{\lambda}_{\mathbf{d}} = \begin{bmatrix} \lambda_{d1} & 0 \\ 0 & \lambda_{d3} \end{bmatrix}, \quad \boldsymbol{\lambda}_{\mathbf{e}} = \begin{bmatrix} \lambda_{e2} & 0 \\ 0 & \lambda_{e4} \end{bmatrix},$$

$$\boldsymbol{\lambda}_{\mathbf{f}} = \begin{bmatrix} \lambda_{f5} & 0 \\ 0 & \lambda_{f6} \end{bmatrix}, \quad \mathbf{H_d} = \begin{bmatrix} H_{d1} & 0 \\ 0 & H_{d3} \end{bmatrix}, \quad \mathbf{H_e} = \begin{bmatrix} H_{e2} & 0 \\ 0 & H_{e4} \end{bmatrix}, \quad \mathbf{H_f} = \begin{bmatrix} H_{f5} & 0 \\ 0 & H_{f6} \end{bmatrix},$$

$$\lambda'_{e2}H_{e2} = \frac{\partial\lambda_2^+}{\partial t}H(t-b_1r_2), \quad \lambda'_{e4}H_{e4} = \frac{\partial\lambda_4^+}{\partial t}H(t-\varepsilon r_2), \quad \lambda'_{d1}H_{d1} = \frac{\partial\lambda_1^+}{\partial t}H(t-t_{1HD}),$$
$$\lambda'_{d3}H_{d1} = \frac{\partial\lambda_7^+}{\partial t}H(t-t_7),$$

$$\lambda'_{d1}H_{d3} = \frac{\partial\lambda_3^+}{\partial t}H(t-t_3), \quad \lambda'_{d3}H_{d3} = \frac{\partial\lambda_8^+}{\partial t}H(t-\varepsilon r_1), \quad \lambda'_{f5}H_{f5} = \frac{\partial\lambda_5^+}{\partial t}H(t-t_{5HD}),$$
$$\lambda'_{f6}H_{f5} = \frac{\partial\lambda_9^+}{\partial t}H(t-t_9),$$

$$\lambda'_{f5}H_{f6} = \frac{\partial\lambda_6^+}{\partial t}H(t-t_6), \quad \lambda'_{f6}H_{f6} = \frac{\partial\lambda_{10}^+}{\partial t}\mathrm{H}(t-\varepsilon r_2), \quad \lambda_{e2}\lambda'_{e2}H_{e2} = \lambda_2^+\frac{\partial\lambda_2^+}{\partial t}H(t-b_1r_2),$$

$$\lambda_{e4}\lambda'_{e4}H_{e4} = \lambda_4^+\frac{\partial\lambda_4^+}{\partial t}H(t-\varepsilon r_2), \quad \lambda_{d1}\lambda'_{d1}H_{d1} = \lambda_1^+\frac{\partial\lambda_1^+}{\partial t}H(t-t_{1HD}), \quad \lambda_{d1}\lambda'_{d3}H_{d1} = \lambda_7^+\frac{\partial\lambda_7^+}{\partial t}H(t-t_7),$$

$$\lambda_{d3}\lambda'_{d1}H_{d3} = \lambda_3^+\frac{\partial\lambda_3^+}{\partial t}H(t-t_3), \quad \lambda_{d3}\lambda'_{d3}H_{d3} = \lambda_8^+\frac{\partial\lambda_8^+}{\partial t}H(t-\varepsilon r_1), \quad \lambda_{f5}\lambda'_{f5}H_{f5} = \lambda_5^+\frac{\partial\lambda_5^+}{\partial t}H(t-t_{5HD}),$$

$$\lambda_{f5}\lambda'_{f6}H_{f5} = \lambda_9^+\frac{\partial\lambda_9^+}{\partial t}H(t-t_9), \quad \lambda_{f6}\lambda'_{f5}H_{f6} = \lambda_6^+\frac{\partial\lambda_6^+}{\partial t}H(t-t_6), \quad \lambda_{f6}\lambda'_{f6}H_{f6} = \lambda_{10}^+\frac{\partial\lambda_{10}^+}{\partial t}\mathrm{H}(t-\varepsilon r_2).$$

3. The existence of surface wave at the piezoelectric bi-material interface

It is important to examine the possibility of surface waves propagating along the interface between piezoelectric bi-materials. We will discuss the existence condition of the surface wave in this section. An explicit expression of the surface wave velocity will be given if the surface wave does exist. The second term of (A.1), which represents the reflected wave, is used to study the surface wave at the interface. The reflected wave is expressed as follows

$$\frac{p}{2\pi}\mathrm{Im}\left[\frac{R_2}{R_1}\frac{\partial\lambda_1^+}{\partial t}\right]\mathrm{H}(t-t_{1HD}), \tag{69}$$

where

$$R_1 = -(e_{15}^{(2)}\varepsilon_{11}^{(1)} - e_{15}^{(1)}\varepsilon_{11}^{(2)})^2\beta(\lambda_1^+) + \bar{c}_{44}^{(1)}\varepsilon_{11}^{(1)}\varepsilon_{11}^{(2)}(\varepsilon_{11}^{(1)} + \varepsilon_{11}^{(2)})\alpha(\lambda_1^+) + \bar{c}_{44}^{(2)}\varepsilon_{11}^{(1)}\varepsilon_{11}^{(2)}(\varepsilon_{11}^{(1)} + \varepsilon_{11}^{(2)})\alpha^*(\lambda_1^+),$$
$$R_2 = (e_{15}^{(2)}\varepsilon_{11}^{(1)} - e_{15}^{(1)}\varepsilon_{11}^{(2)})^2\beta(\lambda_1^+) + \bar{c}_{44}^{(1)}\varepsilon_{11}^{(1)}\varepsilon_{11}^{(2)}(\varepsilon_{11}^{(1)} + \varepsilon_{11}^{(2)})\alpha(\lambda_1^+) - \bar{c}_{44}^{(2)}\varepsilon_{11}^{(1)}\varepsilon_{11}^{(2)}(\varepsilon_{11}^{(1)} + \varepsilon_{11}^{(2)})\alpha^*(\lambda_1^+),$$
$$\beta(\lambda_1^+) = \sqrt{\varepsilon^2 - (\lambda_1^+)^2}, \quad \alpha(\lambda_1^+) = \sqrt{b_1^2 - (\lambda_1^+)^2}, \quad \alpha^*(\lambda_1^+) = \sqrt{b_2^2 - (\lambda_1^+)^2}.$$

The surface wave at the piezoelectric bi-material interface can be constructed by setting the denominator of (69) equal to zero

$$R_1 = -(e_{15}^{(2)}\varepsilon_{11}^{(1)} - e_{15}^{(1)}\varepsilon_{11}^{(2)})^2\beta(\lambda_1^+) + \bar{c}_{44}^{(1)}\varepsilon_{11}^{(1)}\varepsilon_{11}^{(2)}(\varepsilon_{11}^{(1)} + \varepsilon_{11}^{(2)})\alpha(\lambda_1^+) + \bar{c}_{44}^{(2)}\varepsilon_{11}^{(1)}\varepsilon_{11}^{(2)}(\varepsilon_{11}^{(1)} + \varepsilon_{11}^{(2)})\alpha^*(\lambda_1^+) = 0. \tag{70}$$

Note that, (70) is the same as the well-known velocity equation for the MT wave obtained by Maerfeld and Tournois (1971). The number of roots for (70) is determined by means of the principle of the argument (Achenbach, 1976). Let $G_\lambda(z)$ be analytic everywhere inside and on a simple closed curve C_λ, except for a finite number of poles inside C_λ and $G_\lambda(z)$ has no zeros on C_λ. Then

$$\frac{1}{2\pi \mathrm{i}}\int_{C_\lambda} \frac{\mathrm{d}G_\lambda}{\mathrm{d}z}\frac{\mathrm{d}z}{G_\lambda(z)} = Z_\lambda - P_\lambda, \tag{71}$$

where z is a complex variable. Z_λ is the number of zeros inside C_λ and P_λ is the number of poles. The numbers Z_λ and P_λ include the orders of poles and zeros. It is convenient to rewrite (70) in the form

$$R(\lambda) = -(e_{15}^{(2)}\varepsilon_{11}^{(1)} - e_{15}^{(1)}\varepsilon_{11}^{(2)})^2\sqrt{\varepsilon^2 - \lambda^2} + \bar{c}_{44}^{(1)}\varepsilon_{11}^{(1)}\varepsilon_{11}^{(2)}(\varepsilon_{11}^{(1)} + \varepsilon_{11}^{(2)})\sqrt{b_1^2 - \lambda^2} + \bar{c}_{44}^{(2)}\varepsilon_{11}^{(1)}\varepsilon_{11}^{(2)}(\varepsilon_{11}^{(1)} + \varepsilon_{11}^{(2)})\sqrt{b_2^2 - \lambda^2} = 0. \tag{72}$$

In the complex λ-plane, the function $R(\lambda)$ is rendered single-valued by introducing branch cuts. Now consider the contour C_λ consisting of Γ_t, Γ_l and Γ_r as indicated in Fig. 3. Since the function $R(\lambda)$ clearly does not have poles in the complex λ-plane, the number of zeros within the contour $C_\lambda = \Gamma_\mathrm{t} + \Gamma_\mathrm{l} + \Gamma_\mathrm{r}$ is given by

$$Z_\lambda = \frac{1}{2\pi \mathrm{i}}\int_{C_\lambda} \frac{\mathrm{d}R}{\mathrm{d}\lambda}\frac{\mathrm{d}\lambda}{R(\lambda)}. \tag{73}$$

The counting of the number of zeros is carried out by mapping the λ-plane on the v-plane through the relation

$$v = R(\lambda), \quad \mathrm{d}v = \frac{\mathrm{d}R(\lambda)}{\mathrm{d}\lambda}\,\mathrm{d}\lambda. \tag{74}$$

If C_v is the mapping of C_λ in the v-plane, the integral (73) in the v-plane becomes

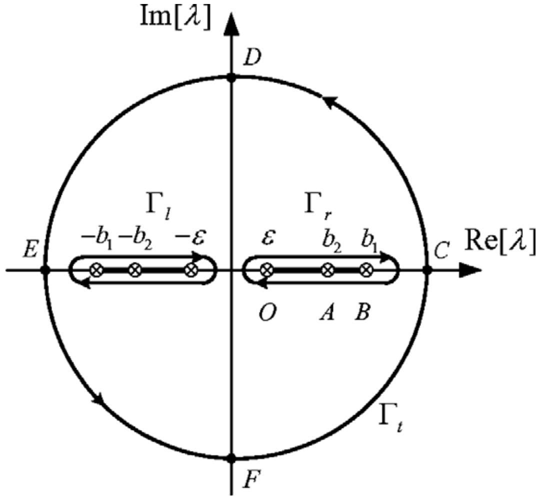

Fig. 3. The λ-plane for $b_1 > b_2$.

$$\frac{1}{2\pi i}\int_{C_v}\frac{dv}{v} = Z_\lambda. \tag{75}$$

The integral in (75) has a simple pole at $v = 0$ and thus the value of Z_λ is simply the number of times the image contour C_v encircles the origin in the v-plane in the counter-clockwise direction. To determine the number of zeros in the λ-plane, we thus carefully trace the mapping of the contour C_λ into the v-plane. Since $R(\lambda) = R(-\lambda)$, the images of Γ_r and Γ_l are the same and only one of them, say Γ_r, needs to be considered.

There are two cases to be discussed, that are $b_1 > b_2$ and $b_2 > b_1$, as follows

Case (a): $b_1 > b_2$ (see Fig. 3).

At O point:

$$R(\varepsilon) = \bar{c}_{44}^{(1)}\varepsilon_{11}^{(1)}\varepsilon_{11}^{(2)}(\varepsilon_{11}^{(1)}+\varepsilon_{11}^{(2)})\sqrt{b_1^2-\varepsilon^2} + \bar{c}_{44}^{(2)}\varepsilon_{11}^{(1)}\varepsilon_{11}^{(2)}(\varepsilon_{11}^{(1)}+\varepsilon_{11}^{(2)})\sqrt{b_2^2-\varepsilon^2}. \tag{76}$$

Along OA:

$$\begin{aligned}R(\lambda) = &\left[\bar{c}_{44}^{(1)}\varepsilon_{11}^{(1)}\varepsilon_{11}^{(2)}(\varepsilon_{11}^{(1)}+\varepsilon_{11}^{(2)})\sqrt{b_1^2-\lambda^2} + \bar{c}_{44}^{(2)}\varepsilon_{11}^{(1)}\varepsilon_{11}^{(2)}(\varepsilon_{11}^{(1)}+\varepsilon_{11}^{(2)})\sqrt{b_2^2-\lambda^2}\right]\\ &\mp\left[-(e_{15}^{(2)}\varepsilon_{11}^{(1)}-e_{15}^{(1)}\varepsilon_{11}^{(2)})^2\sqrt{\lambda^2-\varepsilon^2}\right]i,\end{aligned} \tag{77}$$

where the minus sign applies above the cut and the plus sign applies below the cut.

Also, at A point:

$$R(b_2) = \left[\bar{c}_{44}^{(1)}\varepsilon_{11}^{(1)}\varepsilon_{11}^{(2)}(\varepsilon_{11}^{(1)}+\varepsilon_{11}^{(2)})\sqrt{b_1^2-b_2^2}\right]\mp\left[-(e_{15}^{(2)}\varepsilon_{11}^{(1)}-e_{15}^{(1)}\varepsilon_{11}^{(2)})^2\sqrt{b_2^2-\varepsilon^2}\right]i. \tag{78}$$

Along AB:

$$\begin{aligned}R(\lambda) = &\left[\bar{c}_{44}^{(1)}\varepsilon_{11}^{(1)}\varepsilon_{11}^{(2)}(\varepsilon_{11}^{(1)}+\varepsilon_{11}^{(2)})\sqrt{b_1^2-\lambda^2}\right]\\ &\mp\left[-(e_{15}^{(2)}\varepsilon_{11}^{(1)}-e_{15}^{(1)}\varepsilon_{11}^{(2)})^2\sqrt{\lambda^2-\varepsilon^2} + \bar{c}_{44}^{(2)}\varepsilon_{11}^{(1)}\varepsilon_{11}^{(2)}(\varepsilon_{11}^{(1)}+\varepsilon_{11}^{(2)})\sqrt{\lambda^2-b_2^2}\right]i.\end{aligned} \tag{79}$$

At B point:

$$R(b_1) = \mp\left[-(e_{15}^{(2)}\varepsilon_{11}^{(1)}-e_{15}^{(1)}\varepsilon_{11}^{(2)})^2\sqrt{b_1^2-\varepsilon^2} + \bar{c}_{44}^{(2)}\varepsilon_{11}^{(1)}\varepsilon_{11}^{(2)}(\varepsilon_{11}^{(1)}+\varepsilon_{11}^{(2)})\sqrt{b_1^2-b_2^2}\right]i. \tag{80}$$

For $|\lambda|$ is large, we find

$$R(\lambda) = [-(e_{15}^{(2)}\varepsilon_{11}^{(1)}-e_{15}^{(1)}\varepsilon_{11}^{(2)})^2 + \varepsilon_{11}^{(1)}\varepsilon_{11}^{(2)}(\bar{c}_{44}^{(1)}+\bar{c}_{44}^{(2)})(\varepsilon_{11}^{(1)}+\varepsilon_{11}^{(2)})]\sqrt{-\lambda^2}. \tag{81}$$

Finally, we find that the number of zeros for the function $R(\lambda)$ is mainly controlled by the positive or negative value of the bracket in (80). For the case that

$$-(e_{15}^{(2)}\varepsilon_{11}^{(1)}-e_{15}^{(1)}\varepsilon_{11}^{(2)})^2\sqrt{b_1^2-\varepsilon^2} + \bar{c}_{44}^{(2)}\varepsilon_{11}^{(1)}\varepsilon_{11}^{(2)}(\varepsilon_{11}^{(1)}+\varepsilon_{11}^{(2)})\sqrt{b_1^2-b_2^2} > 0, \tag{82}$$

as indicated in Fig. 4(a), the contours Γ_t, Γ_r and Γ_l in the λ-plane are mapped to the contours Γ_t', Γ_r' and Γ_l' in the v-plane. The contour Γ_t' encircles the origin (pole) counterclockwise in the v-plane and Γ_l' and Γ_r' encircle the origin clockwise in the v-plane.

The contour of Γ_t' is $C' \to D' \to E'$ and $E'' \to F'' \to C''$, and $Z_\lambda = 2\times\frac{1}{2} = 1$.

The contour of Γ_r' is $B' \to A' \to O' \to A'' \to B''$, and $Z_\lambda = -\frac{1}{2}$.

The contour of Γ_l' is the same as the route of Γ_r', and $Z_\lambda = -\frac{1}{2}$.

Hence the number of zeros is zero, i.e. $Z_\lambda = 2\times\frac{1}{2} - 2\times\frac{1}{2} = 0$. For the case that

$$-(e_{15}^{(2)}\varepsilon_{11}^{(1)}-e_{15}^{(1)}\varepsilon_{11}^{(2)})^2\sqrt{b_1^2-\varepsilon^2} + \bar{c}_{44}^{(2)}\varepsilon_{11}^{(1)}\varepsilon_{11}^{(2)}(\varepsilon_{11}^{(1)}+\varepsilon_{11}^{(2)})\sqrt{b_1^2-b_2^2} < 0, \tag{83}$$

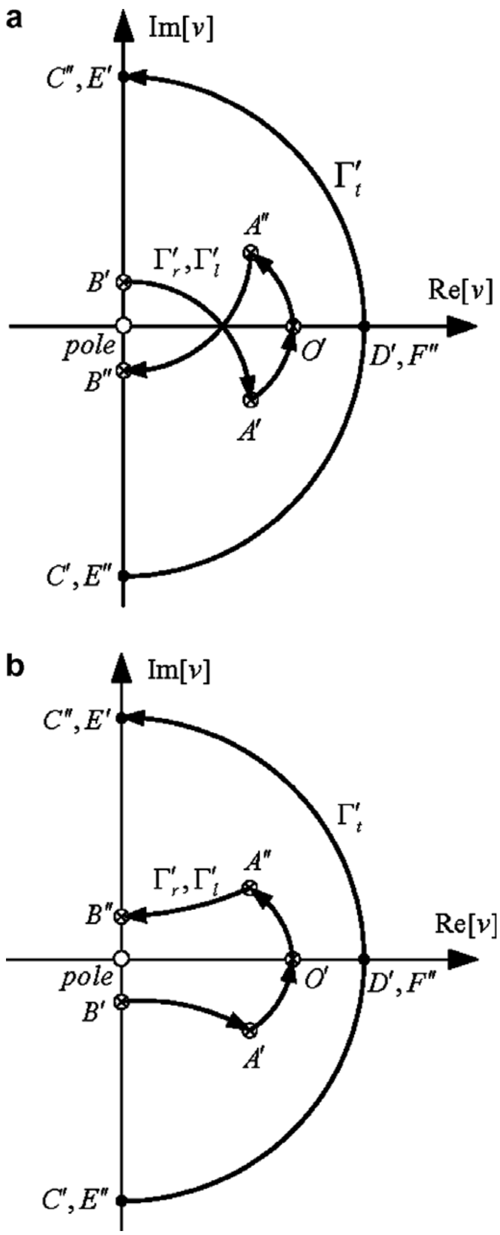

Fig. 4. The v-plane for (a) $\mathrm{Im}[R(b_1)] > 0$ and (b) $\mathrm{Im}[R(b_1)] < 0$.

the contours Γ'_{t}, Γ'_{r} and Γ'_{l} in the v-plane is indicated in Fig. 4(b). The contour Γ'_{t} encircles the origin counterclockwise in the v-plane while Γ'_{l} and Γ'_{r} encircle the origin counterclockwise in the v-plane.

The contour of Γ'_{t} is $C' \to D' \to E'$ and $E'' \to F'' \to C''$, and $Z_\lambda = 2 \times \frac{1}{2} = 1$.

The contour of Γ'_{r} is $B' \to A' \to O' \to A'' \to B''$, and $Z_\lambda = \frac{1}{2}$.

The contour of Γ'_{l} is the same as the route of Γ'_{r}, and $Z_\lambda = \frac{1}{2}$.

Hence the number of zeros for the function $R(\lambda)$ is two, i.e. $Z_\lambda = 2 \times \frac{1}{2} + 2 \times \frac{1}{2} = 2$.

Case (b): $b_2 > b_1$.

At O point:

$$R(\varepsilon) = \bar{c}^{(1)}_{44} \varepsilon^{(1)}_{11} \varepsilon^{(2)}_{11} (\varepsilon^{(1)}_{11} + \varepsilon^{(2)}_{11}) \sqrt{b_1^2 - \varepsilon^2} + \bar{c}^{(2)}_{44} \varepsilon^{(1)}_{11} \varepsilon^{(2)}_{11} (\varepsilon^{(1)}_{11} + \varepsilon^{(2)}_{11}) \sqrt{b_2^2 - \varepsilon^2}. \tag{84}$$

Along OA:

$$R(\lambda)=\left[\bar{c}_{44}^{(1)}\varepsilon_{11}^{(1)}\varepsilon_{11}^{(2)}(\varepsilon_{11}^{(1)}+\varepsilon_{11}^{(2)})\sqrt{b_1^2-\lambda^2}+\bar{c}_{44}^{(2)}\varepsilon_{11}^{(1)}\varepsilon_{11}^{(2)}(\varepsilon_{11}^{(1)}+\varepsilon_{11}^{(2)})\sqrt{b_2^2-\lambda^2}\right] \mp\left[-(e_{15}^{(2)}\varepsilon_{11}^{(1)}-e_{15}^{(1)}\varepsilon_{11}^{(2)})^2\sqrt{\lambda^2-\varepsilon^2}\right]i, \tag{85}$$

where the minus sign applies above the cut and the plus sign applies below the cut.

Also, at A point:

$$R(b_1)=\bar{c}_{44}^{(2)}\varepsilon_{11}^{(1)}\varepsilon_{11}^{(2)}(\varepsilon_{11}^{(1)}+\varepsilon_{11}^{(2)})\sqrt{b_2^2-b_1^2}\mp\left[-(e_{15}^{(2)}\varepsilon_{11}^{(1)}-e_{15}^{(1)}\varepsilon_{11}^{(2)})^2\sqrt{b_1^2-\varepsilon^2}\right]i. \tag{86}$$

Along AB:

$$R(\lambda)=\bar{c}_{44}^{(2)}\varepsilon_{11}^{(1)}\varepsilon_{11}^{(2)}(\varepsilon_{11}^{(1)}+\varepsilon_{11}^{(2)})\sqrt{b_2^2-\lambda^2} \mp\left[-(e_{15}^{(2)}\varepsilon_{11}^{(1)}-e_{15}^{(1)}\varepsilon_{11}^{(2)})^2\sqrt{\lambda^2-\varepsilon^2}+\bar{c}_{44}^{(1)}\varepsilon_{11}^{(1)}\varepsilon_{11}^{(2)}(\varepsilon_{11}^{(1)}+\varepsilon_{11}^{(2)})\sqrt{\lambda^2-b_1^2}\right]i. \tag{87}$$

At B point:

$$R(b_2)=\mp\left[-(e_{15}^{(2)}\varepsilon_{11}^{(1)}-e_{15}^{(1)}\varepsilon_{11}^{(2)})^2\sqrt{b_2^2-\varepsilon^2}+\bar{c}_{44}^{(1)}\varepsilon_{11}^{(1)}\varepsilon_{11}^{(2)}(\varepsilon_{11}^{(1)}+\varepsilon_{11}^{(2)})\sqrt{b_2^2-b_1^2}\right]i. \tag{88}$$

For $|\lambda|$ is large, the result is the same as that indicated in (81). Finally, follow the similar discussion as given in case (a), we find that

$$-(e_{15}^{(2)}\varepsilon_{11}^{(1)}-e_{15}^{(1)}\varepsilon_{11}^{(2)})^2\sqrt{b_2^2-\varepsilon^2}+\bar{c}_{44}^{(1)}\varepsilon_{11}^{(1)}\varepsilon_{11}^{(2)}(\varepsilon_{11}^{(1)}+\varepsilon_{11}^{(2)})\sqrt{b_2^2-b_1^2}>0,\quad Z_\lambda=0, \tag{89}$$

and

$$-(e_{15}^{(2)}\varepsilon_{11}^{(1)}-e_{15}^{(1)}\varepsilon_{11}^{(2)})^2\sqrt{b_2^2-\varepsilon^2}+\bar{c}_{44}^{(1)}\varepsilon_{11}^{(1)}\varepsilon_{11}^{(2)}(\varepsilon_{11}^{(1)}+\varepsilon_{11}^{(2)})\sqrt{b_2^2-b_1^2}<0,\quad Z_\lambda=2. \tag{90}$$

We have shown that the condition for the existence of surface waves is indicated in (83) (or (90)). We will determine the velocity of the surface wave if it exists. Consider the problem that at time $t=0$, a dynamic anti-plane loading is applied at the interface $(x,y)=(0,0)$ and the receiver is located at $(x,\ y)=(x,0)$, then $\sin\theta_1=0$ and $\cos\theta_1=1$. We have

$$\lambda_1^+=-\frac{t}{x}\equiv-\frac{1}{v_s}, \tag{91}$$

where v_s is the surface wave velocity. The solution of v_s in (70) can be obtained and the surface wave velocity is explicitly expressed as

$$v_s=\sqrt{\frac{2D_2}{-E_2-\sqrt{E_2^2-4D_2F_2}}}, \tag{92}$$

where

$$\begin{aligned}
D_2&=[A_2^2-B_2^2],\\
E_2&=[B_2^2(b_1^2+b_2^2)-2A_2C_2],\\
F_2&=[C_2^2-B_2^2b_1^2b_2^2],\\
A_2&=[\varepsilon_{11}^{(1)}\varepsilon_{11}^{(2)}(\varepsilon_{11}^{(1)}+\varepsilon_{11}^{(2)})]^2[(\bar{c}_{44}^{(1)})^2+(\bar{c}_{44}^{(2)})^2]-[e_{15}^{(2)}\varepsilon_{11}^{(1)}-e_{15}^{(1)}\varepsilon_{11}^{(2)}]^4,\\
B_2&=2\bar{c}_{44}^{(1)}\bar{c}_{44}^{(2)}[\varepsilon_{11}^{(1)}\varepsilon_{11}^{(2)}(\varepsilon_{11}^{(1)}+\varepsilon_{11}^{(2)})]^2,\\
C_2&=[\varepsilon_{11}^{(1)}\varepsilon_{11}^{(2)}(\varepsilon_{11}^{(1)}+\varepsilon_{11}^{(2)})]^2[(\bar{c}_{44}^{(1)})^2b_1^2+(\bar{c}_{44}^{(2)})^2b_2^2].
\end{aligned}$$

If the piezoelectric material (2) is reduced to an elastic material, which implies that the piezoelectric effect is neglected and the interface between piezoelectric and elastic bi-material is metallized. The surface wave at the interface between piezoelectric and elastic bi-material is also studied and the result is presented in Appendix B.

If the surface of piezoelectric material (1) is covered with an infinitesimally thin perfect conducting film and the mechanical effect in material (2) is neglected. Then the scalar potential of the electric field is set to be zero on the surface. We have

$$\bar{c}_{44}^{(2)} = 0, \quad e_{15}^{(2)} = 0, \quad \varepsilon_{11}^{(2)} \to \infty. \tag{93}$$

Substitution of (93) into (70) yields

$$\alpha(\lambda_1^+) - k_e^2 \beta(\lambda_1^+) = 0, \tag{94}$$

where $k_e^2 = \frac{(e_{15}^{(1)})^2}{\bar{c}_{44}^{(1)} \varepsilon_{11}^{(1)}}$. By substituting (91) into (94), a simple velocity equation for the electromagneto-acoustic surface wave is obtained as

$$v_s = \sqrt{\frac{\bar{c}_{44}^{(1)}}{\rho^{(1)}}(1 - k_e^4)}. \tag{95}$$

This surface wave velocity recovers the classic BG wave solution. If the surface of piezoelectric material (1) is a free surface, which is in contact with a vacuum half-space on the top, we have

$$\bar{c}_{44}^{(2)} = 0, \quad e_{15}^{(2)} = 0, \quad \varepsilon_{11}^{(2)} = \varepsilon_0. \tag{96}$$

Substitution of (96) into (70) yields

$$\alpha(\lambda_1^+) - k_v^2 \beta(\lambda_1^+) = 0, \tag{97}$$

where $k_v^2 = \frac{(e_{15}^{(1)})^2 \varepsilon_0}{\bar{c}_{44}^{(1)} \varepsilon_{11}^{(1)} (\varepsilon_{11}^{(1)} + \varepsilon_0)}$. Then the electromagneto-acoustic surface wave has the velocity as

$$v_s = \sqrt{\frac{\bar{c}_{44}^{(1)}}{\rho^{(1)}}(1 - k_v^4)}. \tag{98}$$

Once again, we recover the classic result of the classic BG wave solution.

4. Numerical results

With the explicit transient solutions at hand, the numerical calculation of transient response for piezoelectric bi-material subjected to a dynamic anti-plane concentrated force or electric charge is investigated in detail. The correspondent static solutions of the same problem are expressed in Appendix C. At time $t/b_1 r_2 = 0$, the loading is applied suddenly at $(x, y) = (0, d)$ in piezoelectric material (1) as shown in Fig. 1. Table 1 lists the commonly used piezoelectric material properties and correspondent shear wave velocities. There are two cases of piezoelectric bi-material to be considered in this study. One has faster shear wave velocity in material (2) and material (1)–material (2) is PZT4–ZnO. The pattern of wave fronts is shown in Fig. 5 (points A and B are receivers). The transient responses of shear stresses and

Table 1
The material properties and shear wave speeds of piezoelectric materials

	c_{44} (10^{10} N/m^2)	e_{15} (C/m)	ε_{11} (10^{-9} F/m)	ρ (kg/m^3)	$1/b$ (m/s)
ZnO	4.25	−0.48	0.0757	5676	2832.65
PZT4	2.56	12.70	6.4634	7500	2596.26
CdS	1.49	−0.21	0.0799	4824	1789.73
$BaTiO_3$	4.40	11.40	9.8722	5700	3166.83

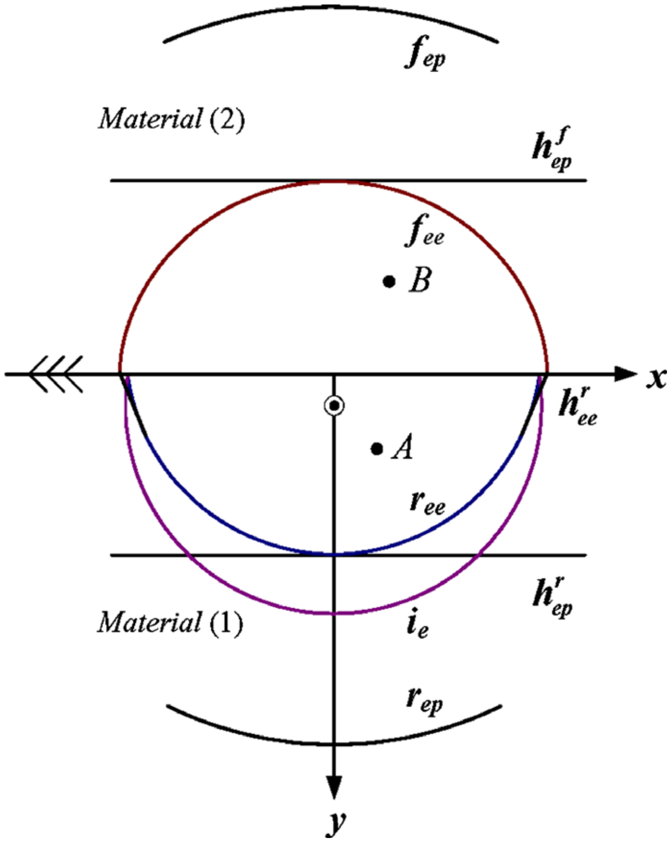

Fig. 5. The pattern of wave fronts for PZT4–ZnO subjected to a dynamic anti-plane concentrated force.

electric displacements for two receivers are presented in Figs. 6–9. The other case has slower shear wave velocity in material (2) and material (1)–material (2) is PZT4–CdS. Similarly, the pattern of wave fronts is shown in Fig. 10 and the transient responses of shear stresses and electric displacements are presented in Figs. 11–14. The waves shown in Figs. 5–14 are composed of incident wave, reflected wave, refracted wave, head wave, elastic wave and electromagnetic wave and are denoted by i, r, f, h, e and p, respectively. For instance, symbol of r_{pe} represents the elastic wave reflected from the interface by the electromagnetic incident wave and symbol of $h^{\mathrm{f}}_{\mathrm{ee}}$ represents the elastic head wave refracted from the interface by the elastic incident wave. It is shown in Figs. 5 and 10 that the wave fronts of head wave are inclined ($h^{\mathrm{r}}_{\mathrm{ee}}$) and horizontal ($h^{\mathrm{r}}_{\mathrm{ep}}$, $h^{\mathrm{f}}_{\mathrm{ep}}$) straight lines for PZT4–ZnO but there is no head wave $h^{\mathrm{r}}_{\mathrm{ee}}$ for PZT4–CdS. The time presented in the transient response curves has been normalized by dividing by $b_1 r_2$. The arrival time for each wave front and the corresponding static values are also indicated in these figures. It is found that the transient responses of shear stresses and electric displacements tend to static value after the arrival of the last wave.

In Fig. 6(a), a small illustration window on the right hand side presents the transient response of $\tau^{(1)}_{yz}$ at time $t/b_1 r_2 = 0$–1. The r_{ep} wave is the first wave arrival at the receiver A at the normalized time equal to 0.5. This wave propagates toward the interface with the elastic wave speed and then travels with the electromagnetic wave velocity after reflected from the interface. It is shown clearly in Fig. 6(a) that the stress field behaves with a square root singularity at the incident i_{e} and reflected r_{ee} wave fronts. However, the contribution of shear stress from r_{ep} and $h^{\mathrm{r}}_{\mathrm{ep}}$ waves is relatively small. In Fig. 6(b), we can see that the only contribution of the electric displacement is due to the r_{ep} wave which is indicated in (A.2). In Fig. 7, the receiver B is located in material (2) and the arrival time of f_{ee} is less than unity because ZnO has faster shear wave velocity than PZT4. In

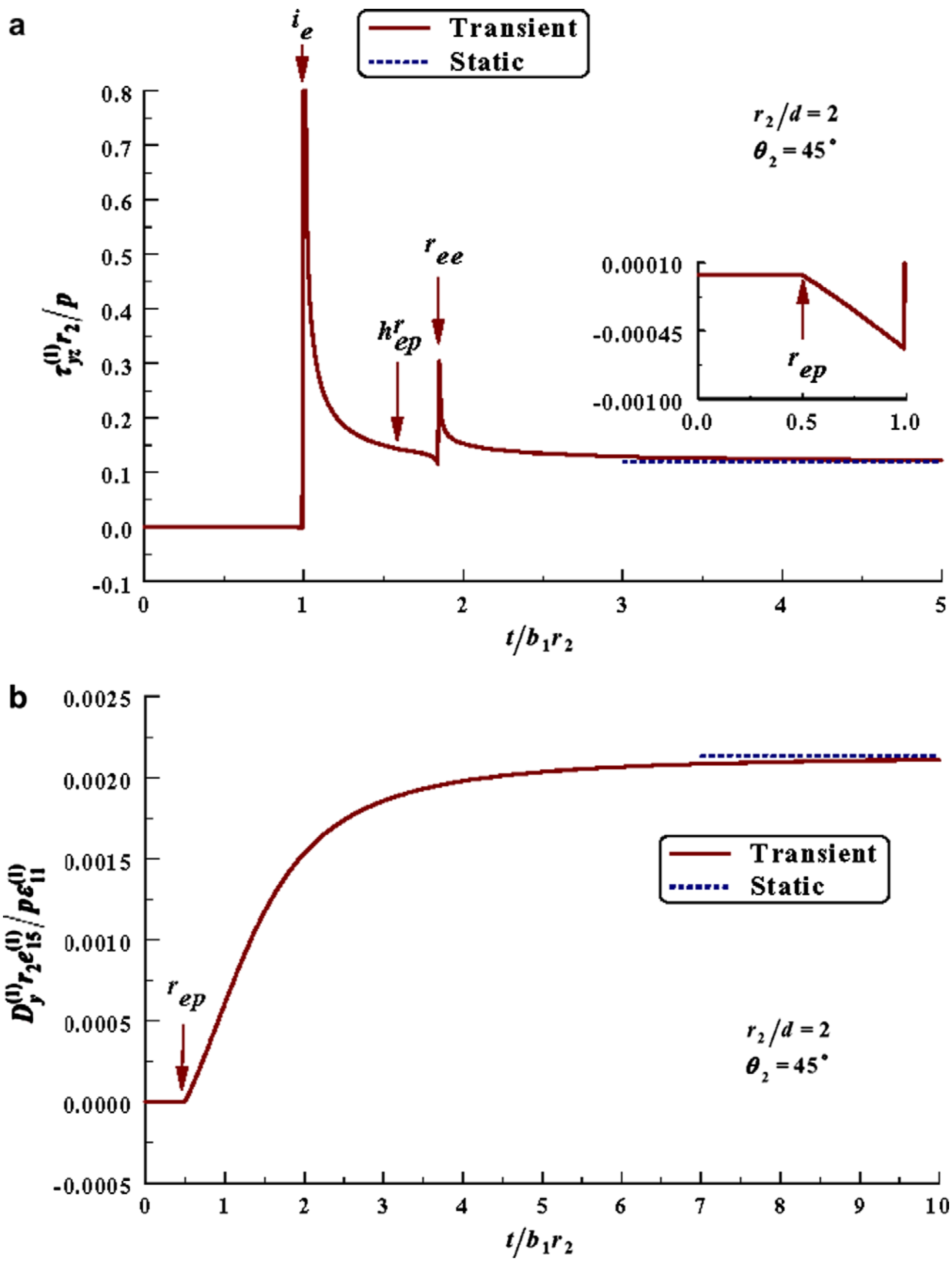

Fig. 6. The transient responses of (a) $\tau^{(1)}_{yz}$ and (b) $D^{(1)}_y$ for PZT4–ZnO subjected to a dynamic anti-plane concentrated force.

order to see the transient response induced by electric loading, a dynamic electric charge in piezoelectric bi-material is considered. In Fig. 8, the transient behavior of shear stress and electric displacement in material (1) are presented and we can see that more waves are generated as compared with Fig. 6. Fig. 9 represent the transient response for material (2). Consequently, it is worthy to note that all kinds of elastic and electro-magnetic waves in piezoelectric bi-material can be generated by applying a dynamic electric charge. For the piezoelectric bi-material is PZT4–CdS, the wave fronts (Fig. 10) for i_e and r_{ee} are circular curves, while f_{ee} wave front is a smooth curve which is constructed by numerical calculations. The transient phenomena in Figs. 11–14 have similar features as that indicated in Figs. 6–9.

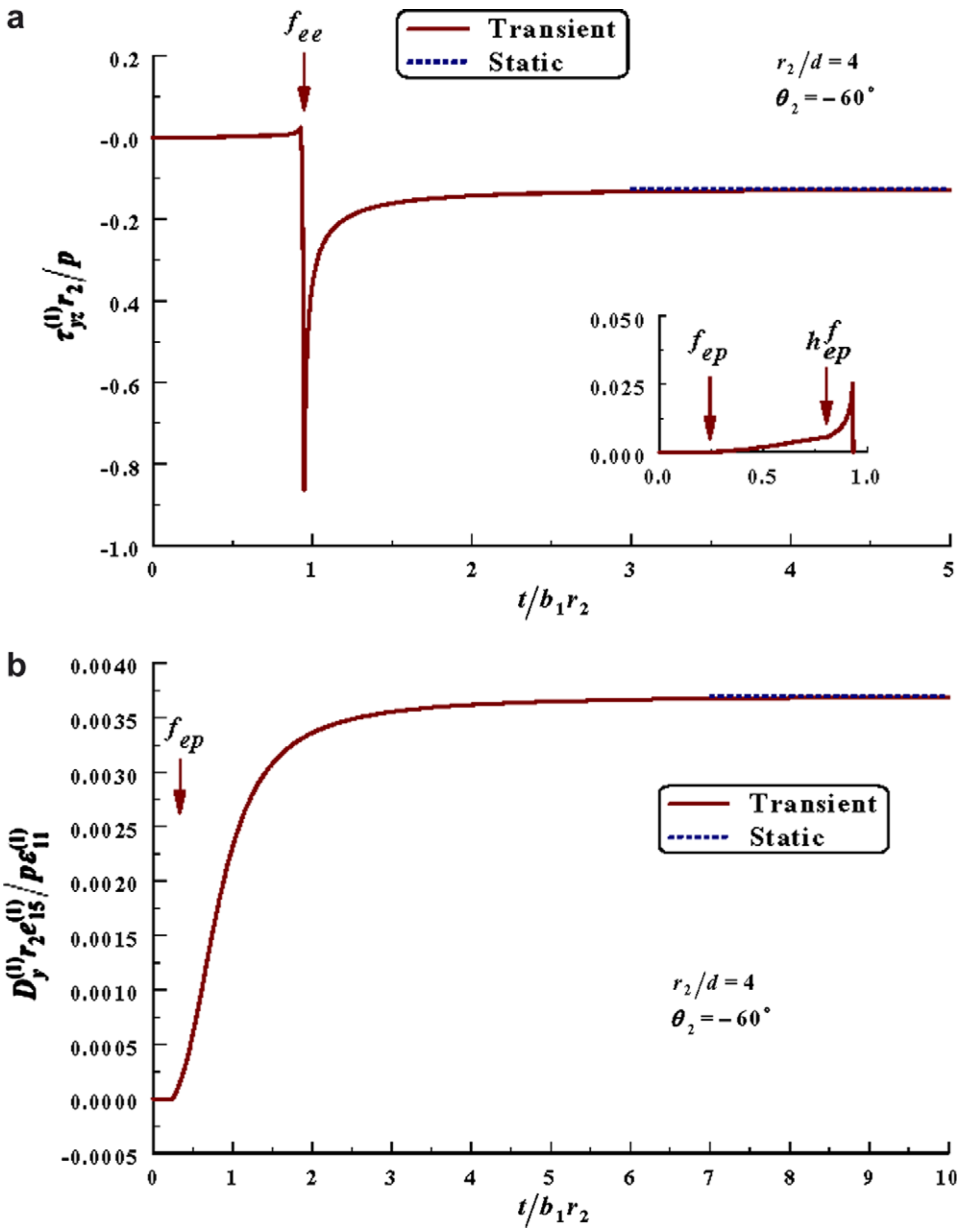

Fig. 7. The transient responses of (a) $\tau_{yz}^{(2)}$ and (b) $D_y^{(2)}$ for PZT4–ZnO subjected to a dynamic anti-plane concentrated force.

The transient solution for applying a dynamic anti-plane concentrated force in a piezoelectric and elastic bi-material can be reduced from the solution for piezoelectric bi-materials. The transient responses of shear stresses for PZT4–Aluminum alloy 2014-T6 and PZT4–Bronze are indicated in Fig. 15 and 16, respectively. Similarly, the transient solutions are shown to approach the correspondent static solutions as time increases. Compared with piezoelectric bi-material, the main distinction is that $\tau_{yz}^{(2)}$ does not have the wave of f_{ep} owing to non-piezoelectricity in material (2). Basically, the transient phenomena as presented in these figures have similar characteristics to those shown in Figs. 6–9.

The existence of surface wave for piezoelectric bi-material for the commonly used material indicated in Table 1 is examined. From the existence condition indicated in (83) (or (90)), it is found that there is no surface

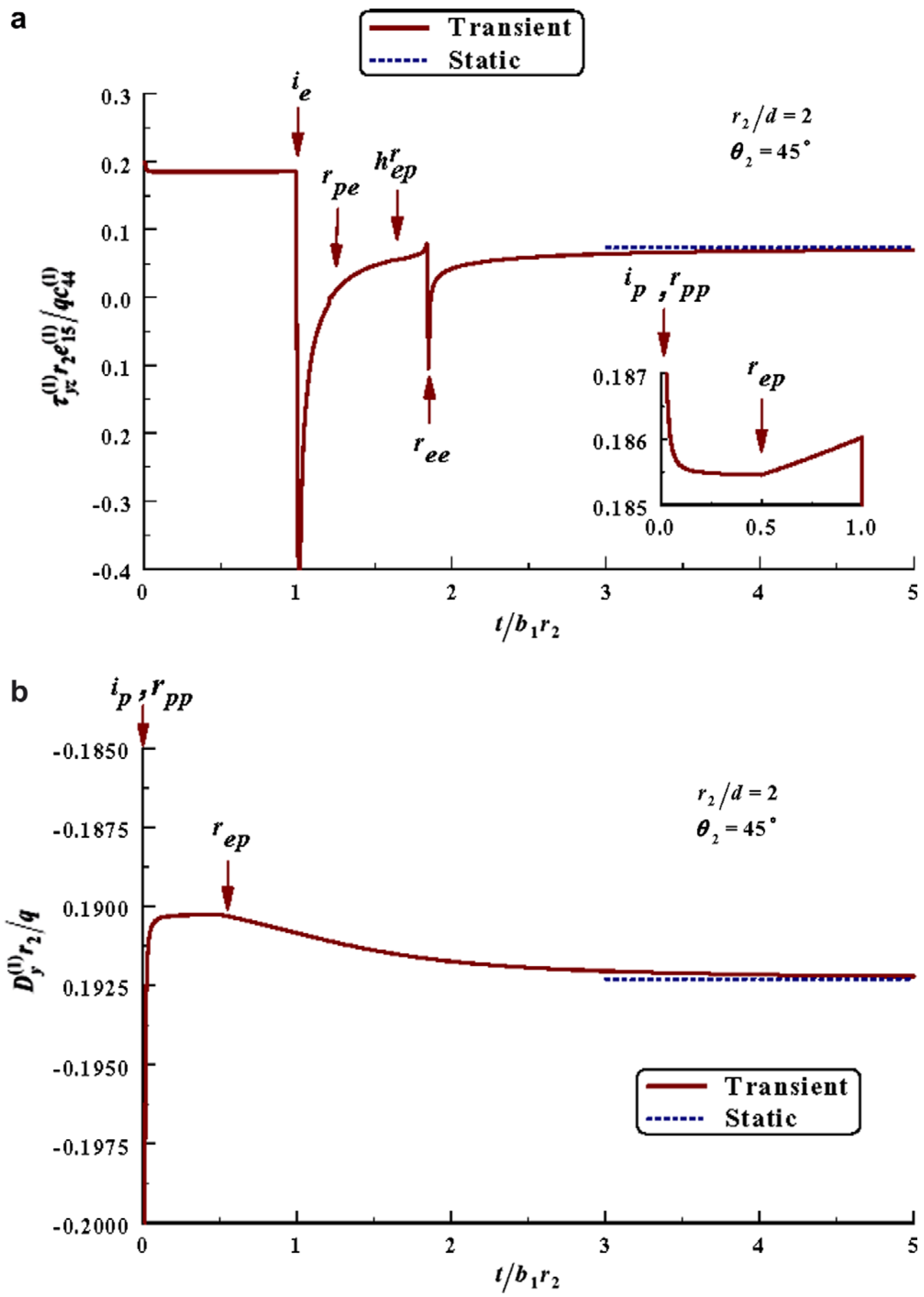

Fig. 8. The transient responses of (a) $\tau_{yz}^{(1)}$ and (b) $D_y^{(1)}$ for PZT4–ZnO subjected to a dynamic electric charge.

wave for any combination of piezoelectric materials listed in Table 1. However, we can not rule out the possibility that there is a surface wave propagating along the interface between piezoelectric bi-material. Hence, we try to investigate if there exist ranges of piezoelectric properties in Table 1 that a surface wave can propagate along the piezoelectric bi-material interface. The virtual piezoelectric material properties are obtained by changing the elastic constant of c_{44} to satisfy (83) (or (90)) and the positive definite conditions. For case (a) ($b_1 > b_2$), the bi-material is PZT4–virtual ZnO, all the material properties are set to be fixed except c_{44} for

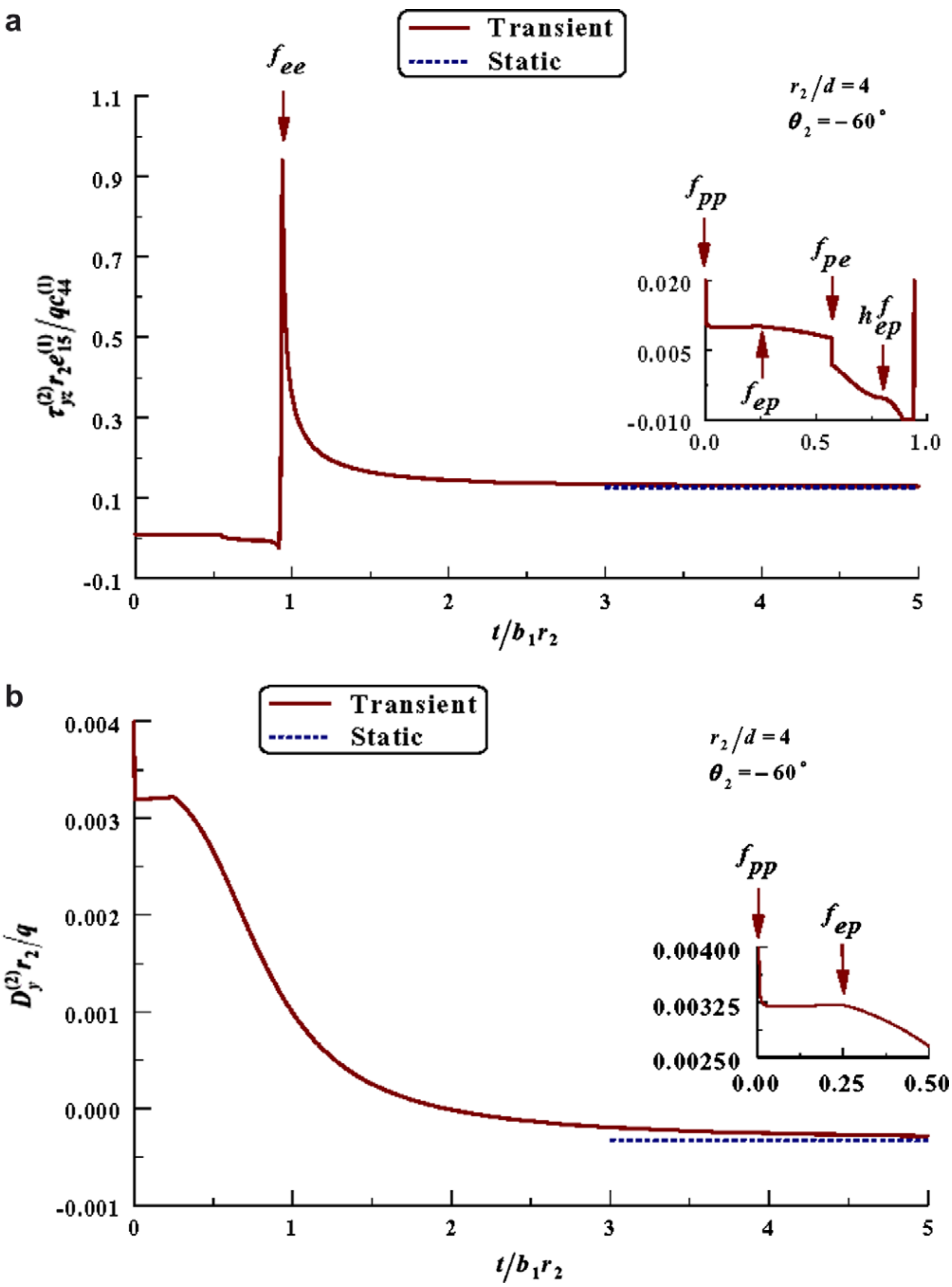

Fig. 9. The transient responses of (a) $\tau_{yz}^{(2)}$ and (b) $D_y^{(2)}$ for PZT4–ZnO subjected to a dynamic electric charge.

ZnO, we find that the existence condition (83) is satisfied only in the range $3.53 \times 10^{10}\ \mathrm{N/m^2} \leqslant c_{44}^{(2)} \leqslant 3.58 \times 10^{10}\ \mathrm{N/m^2}$ (i.e., c_{44} for ZnO is $4.25 \times 10^{10}\ \mathrm{N/m^2}$). The correspondent shear wave speed for *virtual* ZnO is $2599.11\ \mathrm{m/s} \leqslant 1/b_2 \leqslant 2616\ \mathrm{m/s}$. The velocity of the surface wave can be obtained from (92) and the result is $2593\ \mathrm{m/s} \leqslant v_s \leqslant 2596.19\ \mathrm{m/s}$. The shear wave speed for PZT4 is 2596.26 m/s as indicated in Table 1. We can see that the existence of the surface wave only at the situation that the shear wave speed of two materials is close. Furthermore, the surface wave velocity is close to and less than the slower shear wave speed (i.e., PZT4) of the two materials. For case (b) ($b_2 > b_1$), the bi-material is *virtual* $BaTiO_3$–

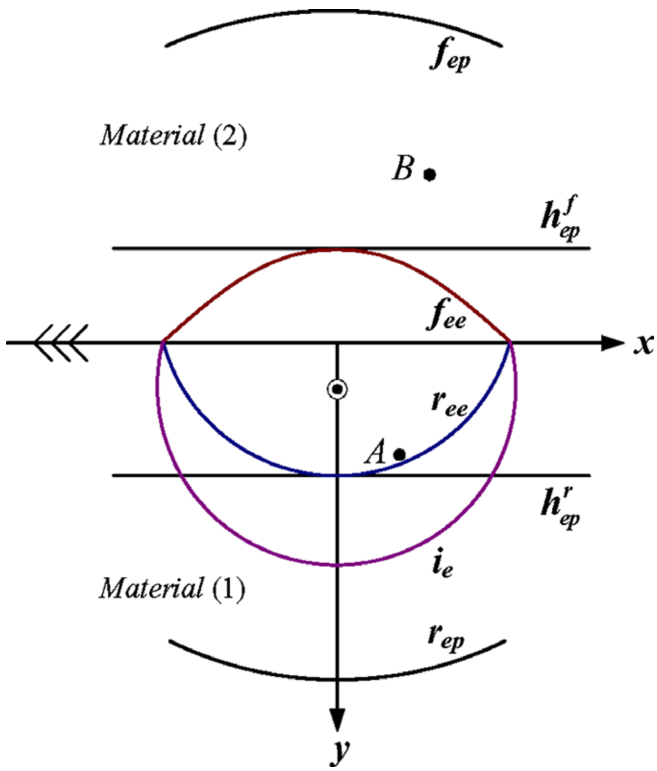

Fig. 10. The pattern of wave fronts for PZT4–CdS subjected to a dynamic anti-plane concentrated force.

ZnO and we change the value of c_{44} for $BaTiO_3$. It is found that the existence condition of surface wave is satisfied only in the range $3.26 \times 10^{10}\ \mathrm{N/m^2} \leqslant c_{44}^{(1)} \leqslant 3.29 \times 10^{10}\ \mathrm{N/m^2}$ (i.e., c_{44} for $BaTiO_3$ is $4.4 \times 10^{10}\ \mathrm{N/m^2}$) and the correspondent shear wave speed for *virtual* $BaTiO_3$ is $2833.52\ \mathrm{m/s} \leqslant 1/b_1 \leqslant 2842.79\ \mathrm{m/s}$. The velocity of the surface wave is $2830.04\ \mathrm{m/s} \leqslant v_s \leqslant 2832.58\ \mathrm{m/s}$. Similar phenomenon in case (a) is found in case (b). The surface wave velocity is close to and less than the slow shear wave speed (i.e., 2832.65 m/s for ZnO).

Table 2 lists the surface wave velocity v_s (if it exists) of the piezoelectric–elastic bi-material which is composed of PZT4 (material (1)) and elastic materials (material (2)). It is interesting to note that the surface wave does exist in the interface of ZnO and nine elastic materials. For example, the surface wave velocity of the bi-material PZT4–Glass is 2595.51 m/s which is slightly less than the shear wave speed of PZT4 (2596.26 m/s). If we change only the elastic constant c_{44} of PZT4 and to find the range of c_{44} such that the surface wave exists, then, we find that there will have a surface wave along the interface of PZT4–Glass bi-material for $2.12 \times 10^{10}\ \mathrm{N/m^2} \leqslant c_{44}^{(1)} \leqslant 6.87 \times 10^{10}\ \mathrm{N/m^2}$ and the surface wave velocity is $2480.71\ \mathrm{m/s} \leqslant v_s \leqslant 3467.1\ \mathrm{m/s}$. For the other case that the elastic material is Bronze, the shear wave speed (2316.43 m/s) is less than that of PZT4. The surface wave velocity is found to be 2313.96 m/s which is slightly less than the shear wave speed of Bronze. The surface wave of PZT4–Bronze exists if c_{44} of PZT4 is in the range of $1.53 \times 10^{10}\ \mathrm{N/m^2} \leqslant c_{44}^{(1)} \leqslant 2.72 \times 10^{10}\ \mathrm{N/m^2}$ and the correspondent surface wave velocity is $2212.64\ \mathrm{m/s} \leqslant v_s \leqslant 2316.43\ \mathrm{m/s}$. We can see from both cases that the range of $c_{44}^{(1)}$ for the existence of the surface wave is much larger than that of piezoelectric bi-materials discussed previously.

For the case that the shear wave speed of the elastic material is larger than that of the piezoelectric material, i.e., $b_1 > b_2'$, the existence condition of the surface wave can be expressed as

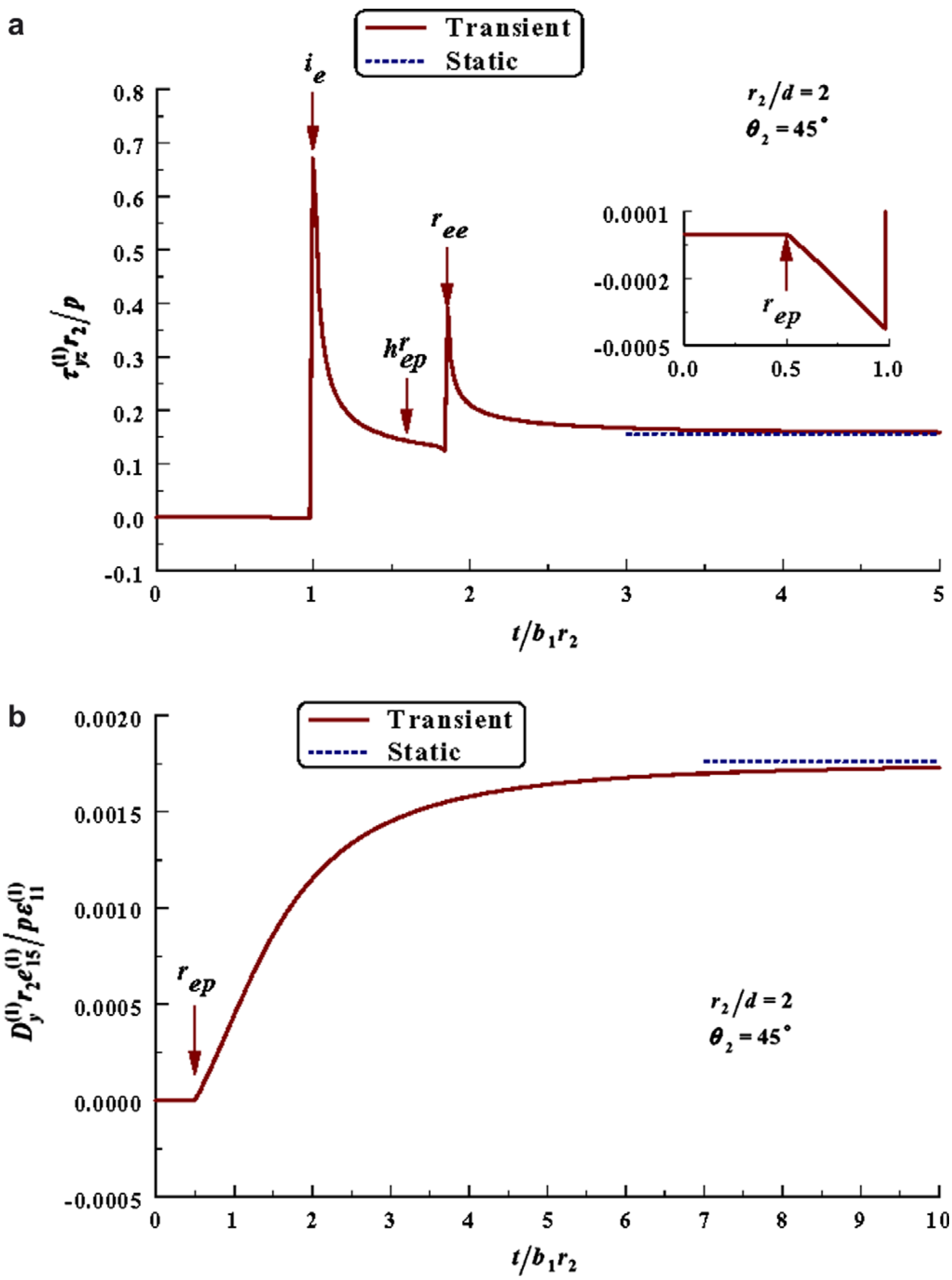

Fig. 11. The transient responses of (a) $\tau_{yz}^{(1)}$ and (b) $D_y^{(1)}$ for PZT4–CdS subjected to a dynamic anti-plane concentrated force.

$$\left[1-\frac{(e_{15}^{(1)})^4}{(\mu\varepsilon_{11}^{(1)})^2}\right]\frac{\mu\rho^{(1)}}{\rho^{(2)}}-\frac{(e_{15}^{(1)})^2}{\varepsilon_{11}^{(1)}}<c_{44}^{(1)}<\frac{\mu\rho^{(1)}}{\rho^{(2)}}-\frac{(e_{15}^{(1)})^2}{\varepsilon_{11}^{(1)}} \text{ and } c_{44}^{(1)}>0. \tag{99}$$

However, if the shear wave speed of the elastic material is less than that of the piezoelectric material, i.e., $b_1<b_2'$, then the condition for the existence of the surface wave becomes

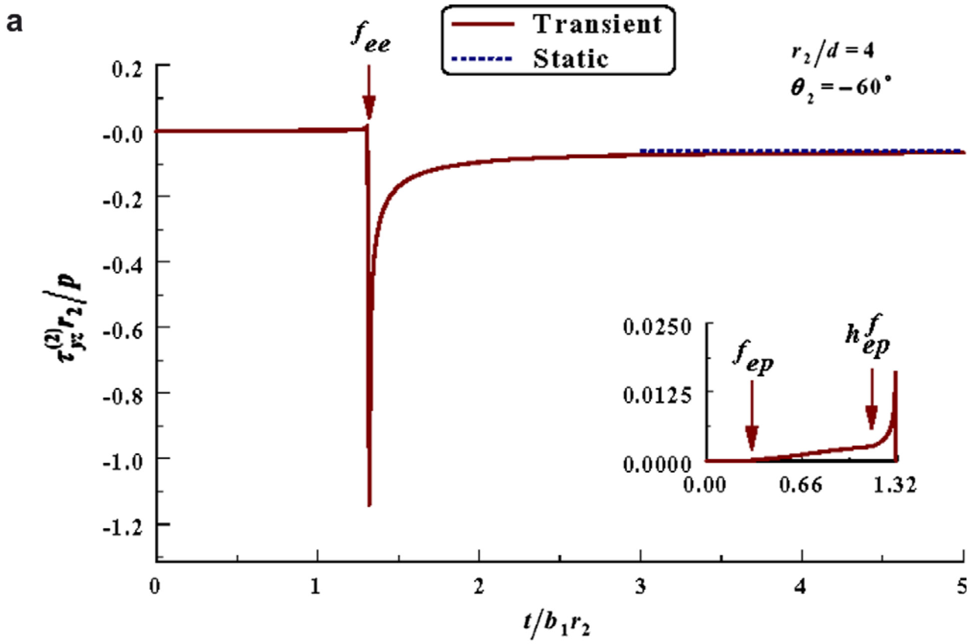

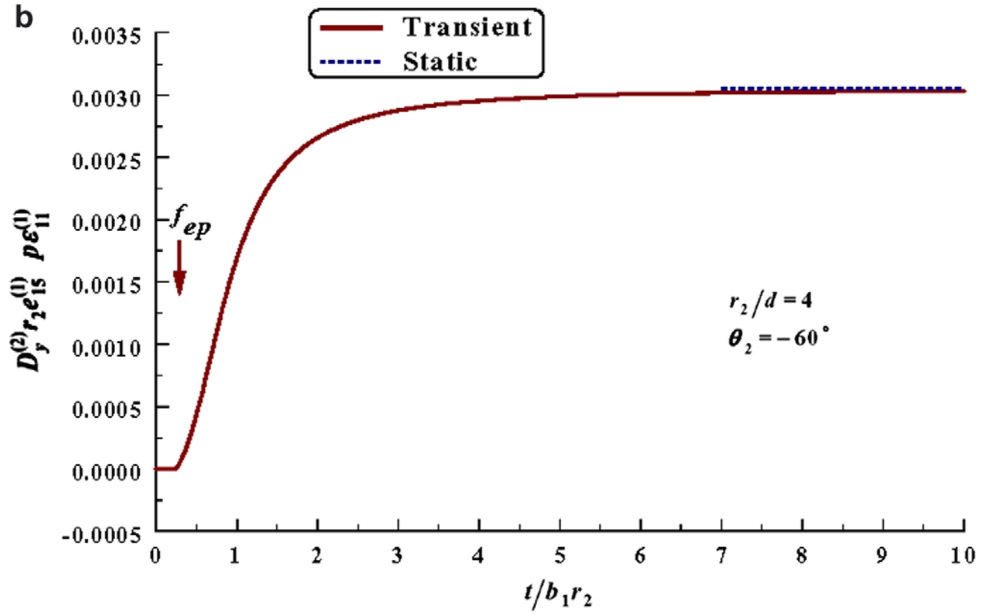

Fig. 12. The transient responses of (a) $\tau_{yz}^{(2)}$ and (b) $D_y^{(2)}$ for PZT4–CdS subjected to a dynamic anti-plane concentrated force.

$$\frac{\mu\rho^{(1)}}{\rho^{(2)}}-\frac{(e_{15}^{(1)})^2}{\varepsilon_{11}^{(1)}}<c_{44}^{(1)}<\frac{\mu\rho^{(1)}}{2\rho^{(2)}}+\sqrt{\left(\frac{\mu\rho^{(1)}}{2\rho^{(2)}}\right)^2+\left(\frac{(e_{15}^{(1)})^2}{\varepsilon_{11}^{(1)}}\right)^2}-\frac{(e_{15}^{(1)})^2}{\varepsilon_{11}^{(1)}}. \tag{100}$$

After the detailed numerical investigation of the existence of the surface wave for piezoelectric–piezoelectric bi-materials and piezoelectric–elastic bi-materials, it can be concluded that the surface wave velocity is always less than the slower shear wave speed of the two materials. Furthermore, the existence of the surface wave for piezoelectric–piezoelectric bi-materials is restricted to the situation that the shear waves of the two piezoelec-

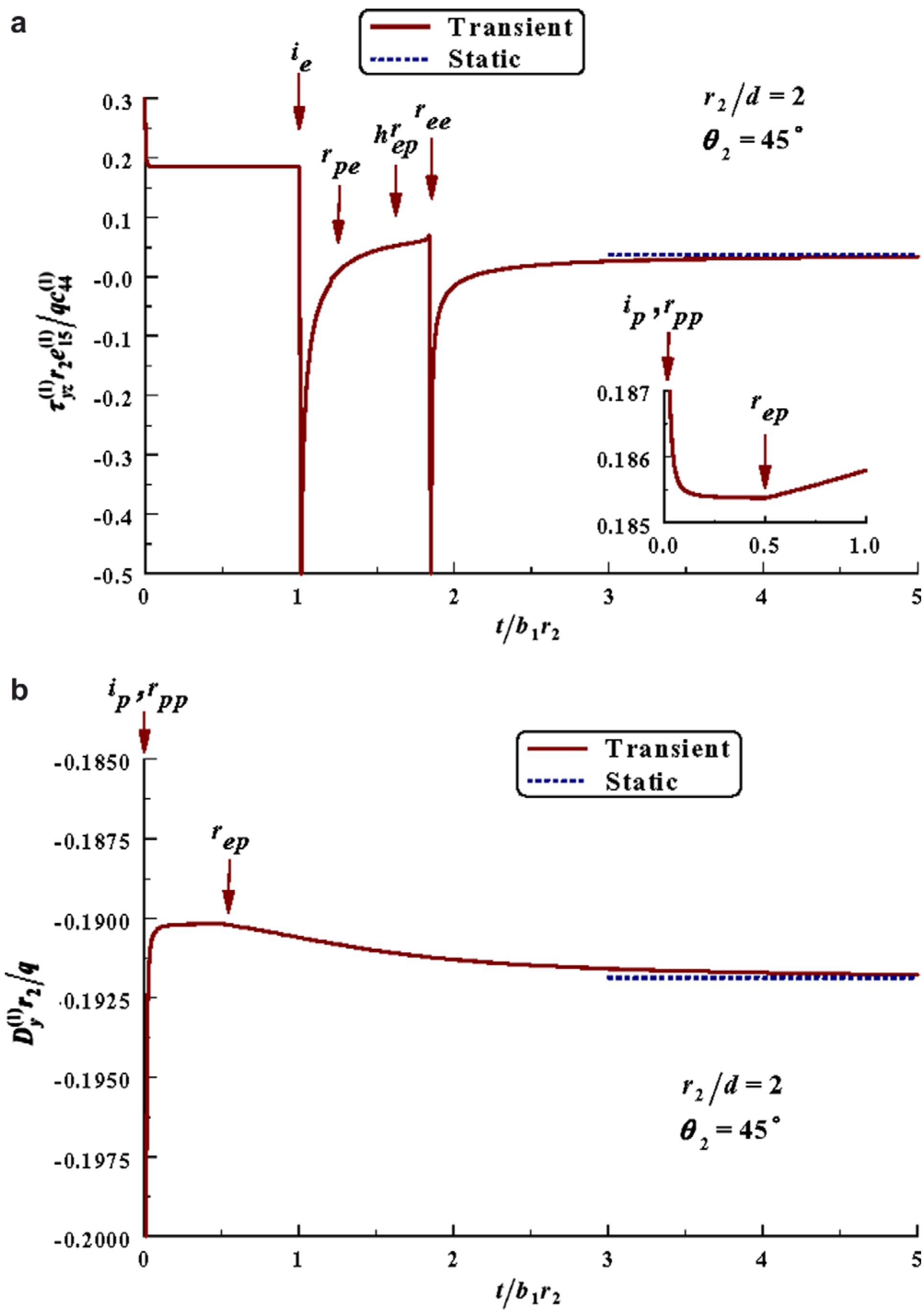

Fig. 13. The transient responses of (a) $\tau_{yz}^{(1)}$ and (b) $D_y^{(1)}$ for PZT4–CdS subjected to a dynamic electric charge.

tric materials are very close. However, the possibility for the existence of the surface wave for piezoelectric–elastic bi-materials is much greater than that of the piezoelectric–piezoelectric bi-materials. In order to present the contribution of surface wave, a material point near the interface between PZT4 and Aluminum alloy 2014-T6 is chosen for investigation. The transient response of a short time interval for the arrival of the surface

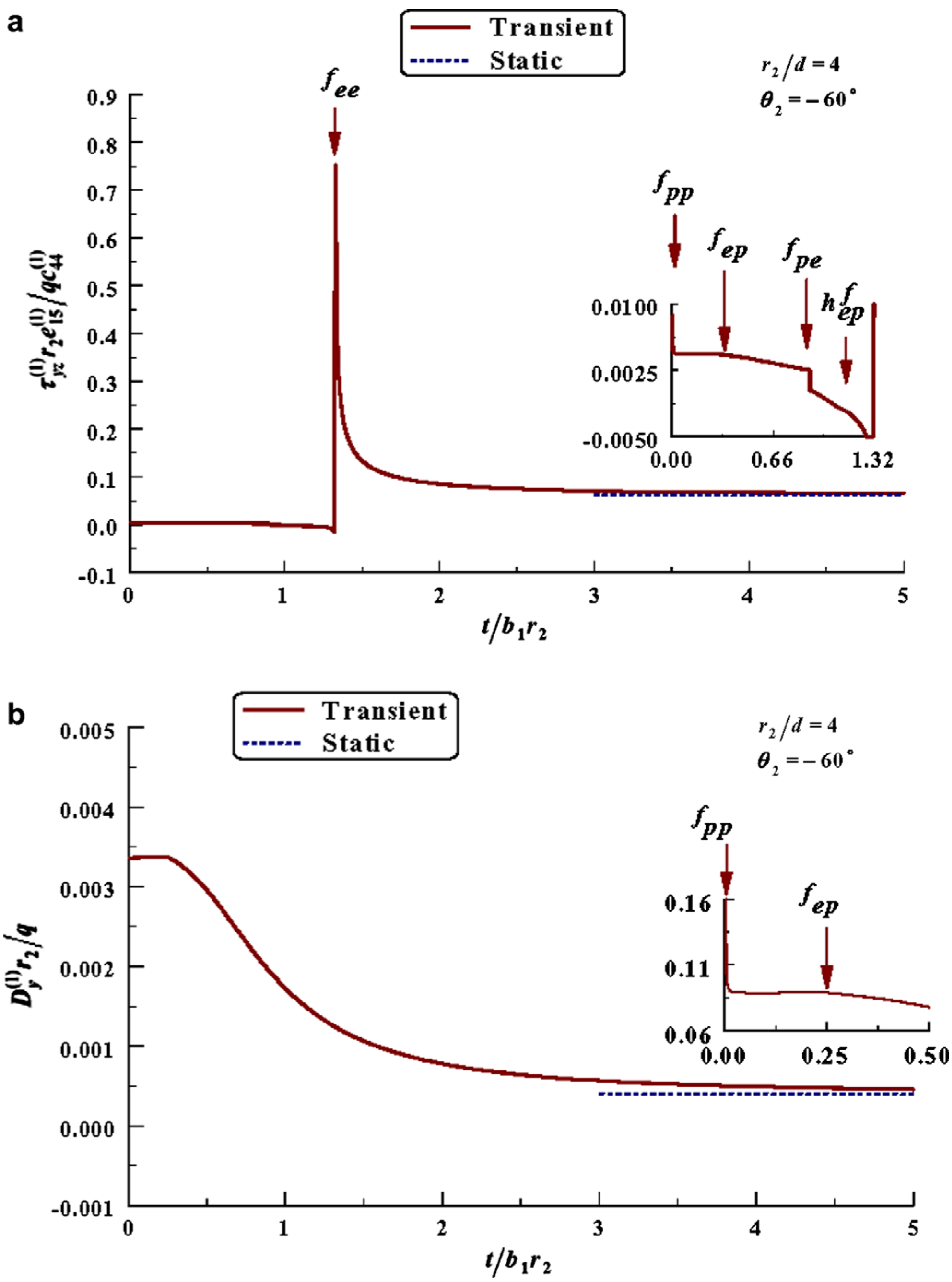

Fig. 14. The transient responses of (a) $\tau_{yz}^{(2)}$ and (b) $D_y^{(2)}$ for PZT4–CdS subjected to a dynamic electric charge.

wave is shown in Fig. 17. Due to the influence of the surface wave, a large variation of shear stress is found in Fig. 17.

5. Conclusion

In this paper, a general methodology is proposed to construct the full-field transient solutions of piezoelectric bi-materials subjected to a dynamic anti-plane concentrated force and a dynamic electric charge.

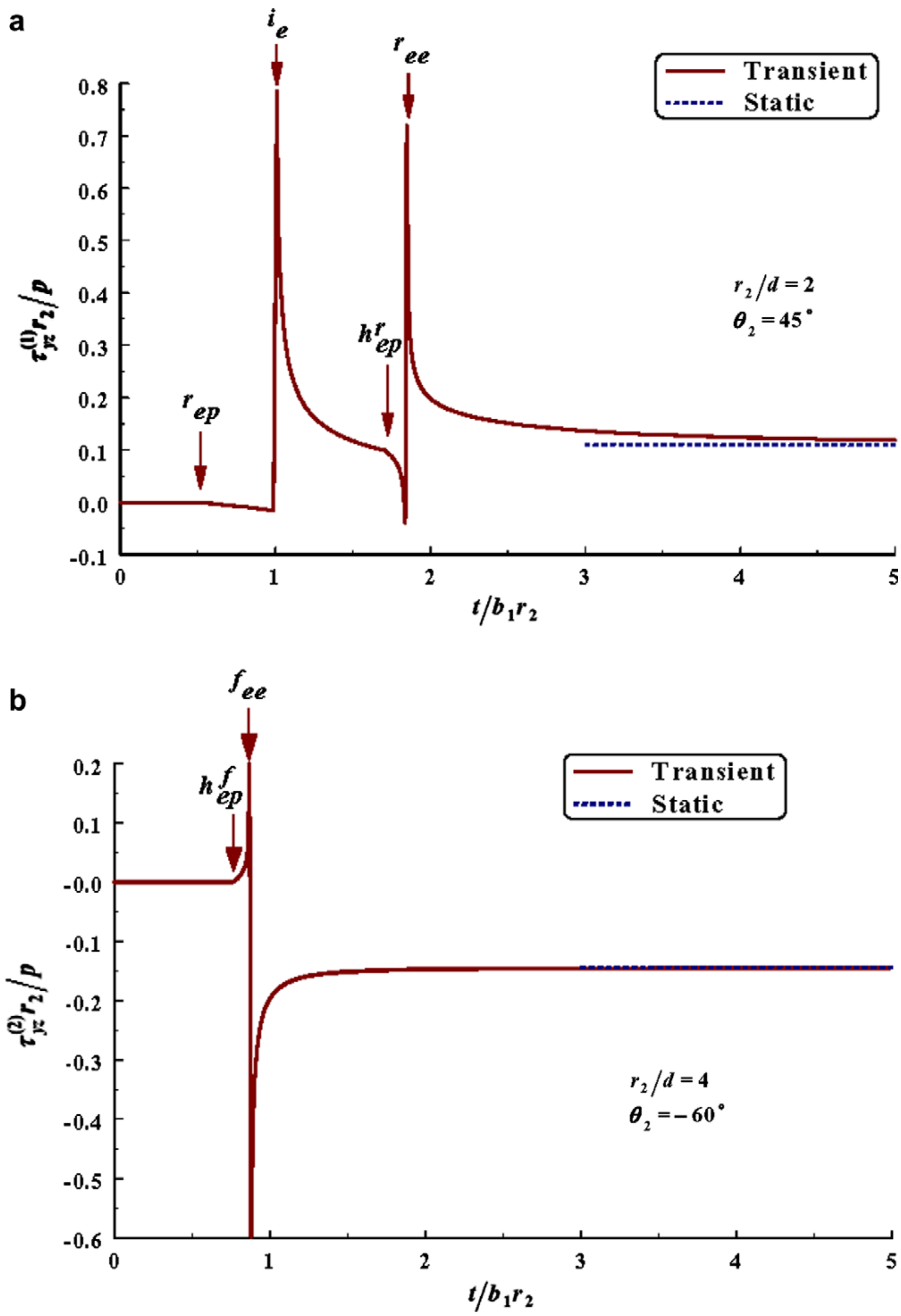

Fig. 15. The transient responses of (a) $\tau^{(1)}_{yz}$ and (b) $\tau^{(2)}_{yz}$ for PZT4–Aluminum alloy 2014-T6 subjected to a dynamic anti-plane concentrated force.

The Cagniard-de Hoop method is used to construct the transient solutions in time domain. The analytical results obtained in this study are exact and are expressed in explicit closed forms, each term representing a physical transient wave. The corresponding static solutions are also obtained in this study. The dynamic response of shear stress in the transient period is much larger than that of the static value. In the transient

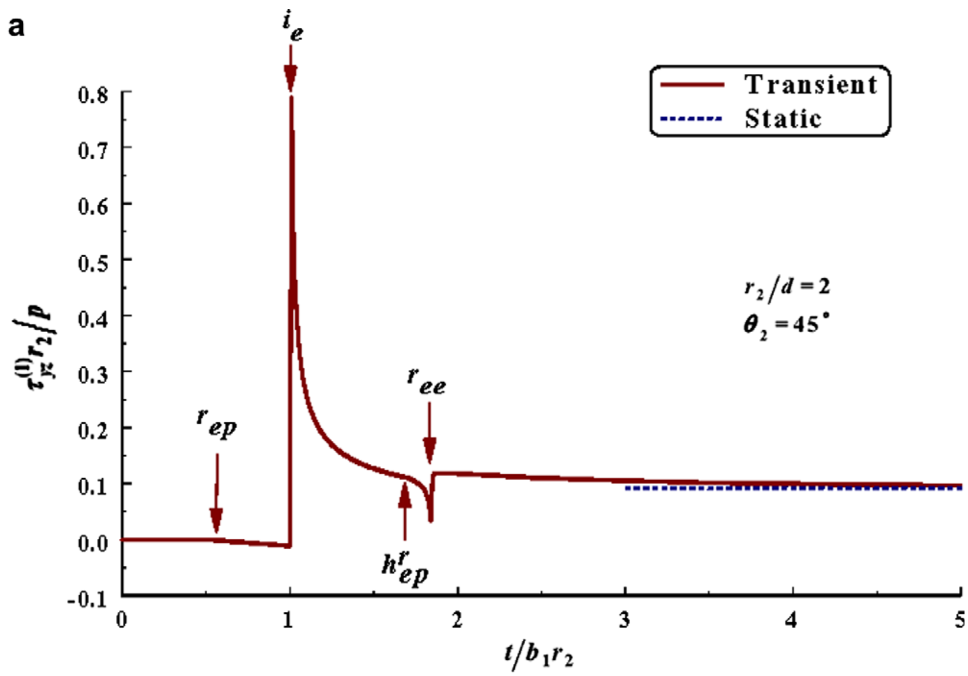

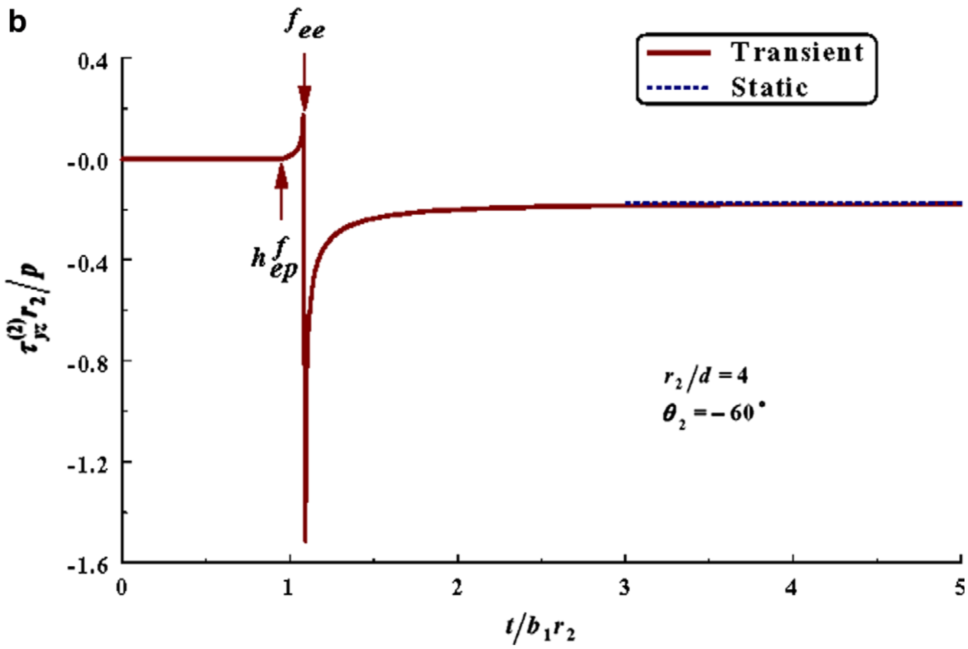

Fig. 16. The transient responses of (a) $\tau^{(1)}_{yz}$ and (b) $\tau^{(2)}_{yz}$ for PZT4–Bronze subjected to a dynamic anti-plane concentrated force.

period, the stress will change radically when the reflected or the refracted wave arrives. The transient value of shear stress will tend toward the static value after the last wave has passed. The existence condition of a surface wave propagating along piezoelectric bi-material interface is established in this study. The velocity of surface wave for the fully-coupled SH electromagneto-acoustic surface wave is obtained in a simple, closed form. It is found in this study that the surface wave velocity is always close to and less than the

Table 2
The material properties of elastic materials and the correspondent surface wave velocities

	μ (10^{10} N/m^2)	ρ (kg/m^3)	$1/b$ (m/s)	v_s (m/s)
Aluminum alloy 2014-T6	2.8	2800	3162.28	2559.25
Aluminum alloy 7075-T6	2.7	2800	3105.30	2549.59
Aluminum alloy 6061-T6	2.6	2700	3103.16	2544.27
Brass	4.1	8400	2209.29	–
Bronze	4.4	8200	2316.43	2313.96
Cast iron	6.9	7200	3095.70	–
Copper and copper alloys	4.7	8900	2298.02	2297.00
Glass	3.5	2800	3535.53	2595.51
Magnesium alloys	1.7	1830	3047.89	2478.38
Monel	6.6	8800	2738.61	2590.00
Nickel	8.0	8800	3015.11	–
Rubber	0.0001	1300	27.74	–
Steel	7.5	7850	3090.98	–
Titanium alloys	3.9	4500	2943.92	2577.25
Tungsten	14.0	1900	8583.95	–

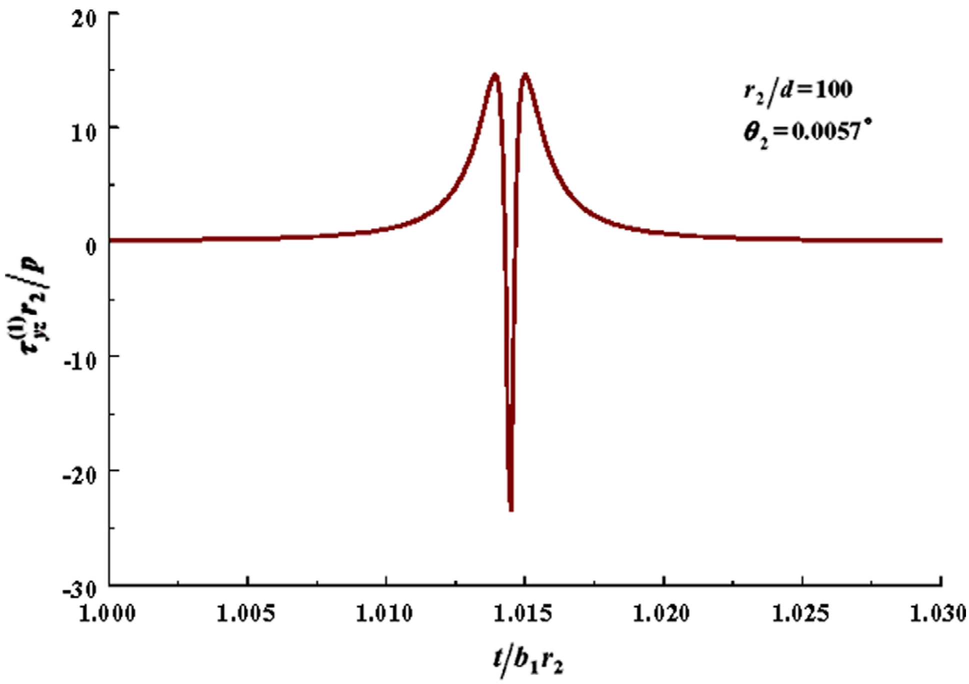

Fig. 17. The transient response of $\tau_{yz}^{(1)}$ at the interface for PZT4–Aluminum alloy 2014-T6 subjected to a dynamic anti-plane concentrated force.

slower shear wave speed of the two materials. Furthermore, the existence of the surface wave for piezoelectric–piezoelectric bi-materials is restricted to the situation that the shear wave speed of the two piezoelectric bi-materials is close.

Acknowledgement

The financial support of the authors from the National Science Council, Republic of China, through Grant NSC 92-2212-E002-074 to National Taiwan University is gratefully acknowledged.

Appendix A

$$\begin{aligned}\tau_{yz}^{(1)} &= \frac{p}{2\pi}\mathrm{Im}\left[\frac{\partial\lambda_2^+}{\partial t}\right]\mathrm{H}(t-b_1r_2)\\&+\frac{p}{2\pi}\mathrm{Im}\left[\frac{\begin{pmatrix}(e_{15}^{(2)}\varepsilon_{11}^{(1)}-e_{15}^{(1)}\varepsilon_{11}^{(2)})^2\beta(\lambda_1^+)+\bar{c}_{44}^{(1)}\varepsilon_{11}^{(1)}\varepsilon_{11}^{(2)}(\varepsilon_{11}^{(1)}+\varepsilon_{11}^{(2)})\alpha(\lambda_1^+)\\-\bar{c}_{44}^{(2)}\varepsilon_{11}^{(1)}\varepsilon_{11}^{(2)}(\varepsilon_{11}^{(1)}+\varepsilon_{11}^{(2)})\alpha^*(\lambda_1^+)\end{pmatrix}}{\begin{pmatrix}-(e_{15}^{(2)}\varepsilon_{11}^{(1)}-e_{15}^{(1)}\varepsilon_{11}^{(2)})^2\beta(\lambda_1^+)+\bar{c}_{44}^{(1)}\varepsilon_{11}^{(1)}\varepsilon_{11}^{(2)}(\varepsilon_{11}^{(1)}+\varepsilon_{11}^{(2)})\alpha(\lambda_1^+)\\+\bar{c}_{44}^{(2)}\varepsilon_{11}^{(1)}\varepsilon_{11}^{(2)}(\varepsilon_{11}^{(1)}+\varepsilon_{11}^{(2)})\alpha^*(\lambda_1^+)\end{pmatrix}}\frac{\partial\lambda_1^+}{\partial t}\right]\mathrm{H}(t-t_{1HD})\\&+\frac{p}{2\pi}\mathrm{Im}\left[\frac{\left(2e_{15}^{(1)}\varepsilon_{11}^{(2)}(e_{15}^{(2)}\varepsilon_{11}^{(1)}-e_{15}^{(1)}\varepsilon_{11}^{(2)})\beta(\lambda_3^+)\right)}{\begin{pmatrix}-(e_{15}^{(2)}\varepsilon_{11}^{(1)}-e_{15}^{(1)}\varepsilon_{11}^{(2)})^2\beta(\lambda_3^+)+\bar{c}_{44}^{(1)}\varepsilon_{11}^{(1)}\varepsilon_{11}^{(2)}(\varepsilon_{11}^{(1)}+\varepsilon_{11}^{(2)})\alpha(\lambda_3^+)\\+\bar{c}_{44}^{(2)}\varepsilon_{11}^{(1)}\varepsilon_{11}^{(2)}(\varepsilon_{11}^{(1)}+\varepsilon_{11}^{(2)})\alpha^*(\lambda_3^+)\end{pmatrix}}\frac{\partial\lambda_3^+}{\partial t}\right]\mathrm{H}(t-t_3),\end{aligned}\tag{A.1}$$

$$D_y^{(1)}=\frac{-p}{2\pi}\mathrm{Im}\left[\frac{\left(2\varepsilon_{11}^{(1)}\varepsilon_{11}^{(2)}(e_{15}^{(2)}\varepsilon_{11}^{(1)}-e_{15}^{(1)}\varepsilon_{11}^{(2)})\beta(\lambda_3^+)\right)}{\begin{pmatrix}-(e_{15}^{(2)}\varepsilon_{11}^{(1)}-e_{15}^{(1)}\varepsilon_{11}^{(2)})^2\beta(\lambda_3^+)+\bar{c}_{44}^{(1)}\varepsilon_{11}^{(1)}\varepsilon_{11}^{(2)}(\varepsilon_{11}^{(1)}+\varepsilon_{11}^{(2)})\alpha(\lambda_3^+)\\+\bar{c}_{44}^{(2)}\varepsilon_{11}^{(1)}\varepsilon_{11}^{(2)}(\varepsilon_{11}^{(1)}+\varepsilon_{11}^{(2)})\alpha^*(\lambda_3^+)\end{pmatrix}}\frac{\partial\lambda_3^+}{\partial t}\right]\mathrm{H}(t-t_3),\tag{A.2}$$

$$\begin{aligned}\tau_{xz}^{(1)} &= \frac{p}{2\pi}\mathrm{Im}\left[\frac{\lambda_2^+}{\alpha(\lambda_2^+)}\frac{\partial\lambda_2^+}{\partial t}\right]\mathrm{H}(t-b_1r_2)\\&+\frac{p}{2\pi}\mathrm{Im}\left[\frac{\lambda_1^+\begin{pmatrix}(e_{15}^{(2)}\varepsilon_{11}^{(1)}-e_{15}^{(1)}\varepsilon_{11}^{(2)})^2\beta(\lambda_1^+)+\bar{c}_{44}^{(1)}\varepsilon_{11}^{(1)}\varepsilon_{11}^{(2)}(\varepsilon_{11}^{(1)}+\varepsilon_{11}^{(2)})\alpha(\lambda_1^+)\\-\bar{c}_{44}^{(2)}\varepsilon_{11}^{(1)}\varepsilon_{11}^{(2)}(\varepsilon_{11}^{(1)}+\varepsilon_{11}^{(2)})\alpha^*(\lambda_1^+)\end{pmatrix}}{\alpha(\lambda_1^+)\begin{pmatrix}-(e_{15}^{(2)}\varepsilon_{11}^{(1)}-e_{15}^{(1)}\varepsilon_{11}^{(2)})^2\beta(\lambda_1^+)+\bar{c}_{44}^{(1)}\varepsilon_{11}^{(1)}\varepsilon_{11}^{(2)}(\varepsilon_{11}^{(1)}+\varepsilon_{11}^{(2)})\alpha(\lambda_1^+)\\+\bar{c}_{44}^{(2)}\varepsilon_{11}^{(1)}\varepsilon_{11}^{(2)}(\varepsilon_{11}^{(1)}+\varepsilon_{11}^{(2)})\alpha^*(\lambda_1^+)\end{pmatrix}}\frac{\partial\lambda_1^+}{\partial t}\right]\mathrm{H}(t-t_{1HD})\\&+\frac{p}{2\pi}\mathrm{Im}\left[\frac{\left(2e_{15}^{(1)}\varepsilon_{11}^{(2)}(e_{15}^{(2)}\varepsilon_{11}^{(1)}-e_{15}^{(1)}\varepsilon_{11}^{(2)})\lambda_3^+\right)}{\begin{pmatrix}-(e_{15}^{(2)}\varepsilon_{11}^{(1)}-e_{15}^{(1)}\varepsilon_{11}^{(2)})^2\beta(\lambda_3^+)+\bar{c}_{44}^{(1)}\varepsilon_{11}^{(1)}\varepsilon_{11}^{(2)}(\varepsilon_{11}^{(1)}+\varepsilon_{11}^{(2)})\alpha(\lambda_3^+)\\+\bar{c}_{44}^{(2)}\varepsilon_{11}^{(1)}\varepsilon_{11}^{(2)}(\varepsilon_{11}^{(1)}+\varepsilon_{11}^{(2)})\alpha^*(\lambda_3^+)\end{pmatrix}}\frac{\partial\lambda_3^+}{\partial t}\right]\mathrm{H}(t-t_3),\end{aligned}\tag{A.3}$$

$$D_x^{(1)}=\frac{p}{2\pi}\mathrm{Im}\left[\frac{\left(2\varepsilon_{11}^{(1)}\varepsilon_{11}^{(2)}(e_{15}^{(2)}\varepsilon_{11}^{(1)}-e_{15}^{(1)}\varepsilon_{11}^{(2)})\lambda_3^+\right)}{\begin{pmatrix}-(e_{15}^{(2)}\varepsilon_{11}^{(1)}-e_{15}^{(1)}\varepsilon_{11}^{(2)})^2\beta(\lambda_3^+)+\bar{c}_{44}^{(1)}\varepsilon_{11}^{(1)}\varepsilon_{11}^{(2)}(\varepsilon_{11}^{(1)}+\varepsilon_{11}^{(2)})\alpha(\lambda_3^+)\\+\bar{c}_{44}^{(2)}\varepsilon_{11}^{(1)}\varepsilon_{11}^{(2)}(\varepsilon_{11}^{(1)}+\varepsilon_{11}^{(2)})\alpha^*(\lambda_3^+)\end{pmatrix}}\frac{\partial\lambda_3^+}{\partial t}\right]\mathrm{H}(t-t_3),\tag{A.4}$$

$$\begin{aligned}\tau_{yz}^{(2)} &= \frac{-p}{2\pi}\mathrm{Im}\left[\frac{\left(2\bar{c}_{44}^{(2)}\varepsilon_{11}^{(1)}\varepsilon_{11}^{(2)}(\varepsilon_{11}^{(1)}+\varepsilon_{11}^{(2)})\alpha^*(\lambda_5^+)\right)}{\begin{pmatrix}-(e_{15}^{(2)}\varepsilon_{11}^{(1)}-e_{15}^{(1)}\varepsilon_{11}^{(2)})^2\beta(\lambda_5^+)+\bar{c}_{44}^{(1)}\varepsilon_{11}^{(1)}\varepsilon_{11}^{(2)}(\varepsilon_{11}^{(1)}+\varepsilon_{11}^{(2)})\alpha(\lambda_5^+)\\+\bar{c}_{44}^{(2)}\varepsilon_{11}^{(1)}\varepsilon_{11}^{(2)}(\varepsilon_{11}^{(1)}+\varepsilon_{11}^{(2)})\alpha^*(\lambda_5^+)\end{pmatrix}}\frac{\partial\lambda_5^+}{\partial t}\right]\mathrm{H}(t-t_{5HD})\\&-\frac{p}{2\pi}\mathrm{Im}\left[\frac{\left(2e_{15}^{(2)}\varepsilon_{11}^{(1)}(e_{15}^{(1)}\varepsilon_{11}^{(2)}-e_{15}^{(2)}\varepsilon_{11}^{(1)})\beta(\lambda_6^+)\right)}{\begin{pmatrix}-(e_{15}^{(2)}\varepsilon_{11}^{(1)}-e_{15}^{(1)}\varepsilon_{11}^{(2)})^2\beta(\lambda_6^+)+\bar{c}_{44}^{(1)}\varepsilon_{11}^{(1)}\varepsilon_{11}^{(2)}(\varepsilon_{11}^{(1)}+\varepsilon_{11}^{(2)})\alpha(\lambda_6^+)\\+\bar{c}_{44}^{(2)}\varepsilon_{11}^{(1)}\varepsilon_{11}^{(2)}(\varepsilon_{11}^{(1)}+\varepsilon_{11}^{(2)})\alpha^*(\lambda_6^+)\end{pmatrix}}\frac{\partial\lambda_6^+}{\partial t}\right]\mathrm{H}(t-t_6),\end{aligned}\tag{A.5}$$

$$D_y^{(2)} = \frac{-p}{2\pi}\mathrm{Im}\left[\frac{\left(2\varepsilon_{11}^{(1)}\varepsilon_{11}^{(2)}(e_{15}^{(2)}\varepsilon_{11}^{(1)} - e_{15}^{(1)}\varepsilon_{11}^{(2)})\beta(\lambda_6^+)\right)}{\begin{pmatrix}-(e_{15}^{(2)}\varepsilon_{11}^{(1)} - e_{15}^{(1)}\varepsilon_{11}^{(2)})^2\beta(\lambda_6^+) + \bar{c}_{44}^{(1)}\varepsilon_{11}^{(1)}\varepsilon_{11}^{(2)}(\varepsilon_{11}^{(1)} + \varepsilon_{11}^{(2)})\alpha(\lambda_6^+)\\ +\bar{c}_{44}^{(2)}\varepsilon_{11}^{(1)}\varepsilon_{11}^{(2)}(\varepsilon_{11}^{(1)} + \varepsilon_{11}^{(2)})\alpha^*(\lambda_6^+)\end{pmatrix}}\frac{\partial\lambda_6^+}{\partial t}\right]\mathrm{H}(t - t_6), \tag{A.6}$$

$$\begin{aligned}\tau_{xz}^{(2)} = {} & \frac{-p}{2\pi}\mathrm{Im}\left[\frac{\left(2\bar{c}_{44}^{(2)}\varepsilon_{11}^{(1)}\varepsilon_{11}^{(2)}(\varepsilon_{11}^{(1)} + \varepsilon_{11}^{(2)})\lambda_5^+\right)}{\begin{pmatrix}-(e_{15}^{(2)}\varepsilon_{11}^{(1)} - e_{15}^{(1)}\varepsilon_{11}^{(2)})^2\beta(\lambda_5^+) + \bar{c}_{44}^{(1)}\varepsilon_{11}^{(1)}\varepsilon_{11}^{(2)}(\varepsilon_{11}^{(1)} + \varepsilon_{11}^{(2)})\alpha(\lambda_5^+)\\ +\bar{c}_{44}^{(2)}\varepsilon_{11}^{(1)}\varepsilon_{11}^{(2)}(\varepsilon_{11}^{(1)} + \varepsilon_{11}^{(2)})\alpha^*(\lambda_5^+)\end{pmatrix}}\frac{\partial\lambda_5^+}{\partial t}\right]\mathrm{H}(t - t_{5HD})\\ & - \frac{p}{2\pi}\mathrm{Im}\left[\frac{\left(2e_{15}^{(2)}\varepsilon_{11}^{(1)}(e_{15}^{(1)}\varepsilon_{11}^{(2)} - e_{15}^{(2)}\varepsilon_{11}^{(1)})\lambda_6^+\right)}{\begin{pmatrix}-(e_{15}^{(2)}\varepsilon_{11}^{(1)} - e_{15}^{(1)}\varepsilon_{11}^{(2)})^2\beta(\lambda_6^+) + \bar{c}_{44}^{(1)}\varepsilon_{11}^{(1)}\varepsilon_{11}^{(2)}(\varepsilon_{11}^{(1)} + \varepsilon_{11}^{(2)})\alpha(\lambda_6^+)\\ +\bar{c}_{44}^{(2)}\varepsilon_{11}^{(1)}\varepsilon_{11}^{(2)}(\varepsilon_{11}^{(1)} + \varepsilon_{11}^{(2)})\alpha^*(\lambda_6^+)\end{pmatrix}}\frac{\partial\lambda_6^+}{\partial t}\right]\mathrm{H}(t - t_6),\end{aligned} \tag{A.7}$$

$$D_x^{(2)} = \frac{-p}{2\pi}\mathrm{Im}\left[\frac{\left(2\varepsilon_{11}^{(1)}\varepsilon_{11}^{(2)}(e_{15}^{(2)}\varepsilon_{11}^{(1)} - e_{15}^{(1)}\varepsilon_{11}^{(2)})\lambda_6^+\right)}{\begin{pmatrix}-(e_{15}^{(2)}\varepsilon_{11}^{(1)} - e_{15}^{(1)}\varepsilon_{11}^{(2)})^2\beta(\lambda_6^+) + \bar{c}_{44}^{(1)}\varepsilon_{11}^{(1)}\varepsilon_{11}^{(2)}(\varepsilon_{11}^{(1)} + \varepsilon_{11}^{(2)})\alpha(\lambda_6^+)\\ +\bar{c}_{44}^{(2)}\varepsilon_{11}^{(1)}\varepsilon_{11}^{(2)}(\varepsilon_{11}^{(1)} + \varepsilon_{11}^{(2)})\alpha^*(\lambda_6^+)\end{pmatrix}}\frac{\partial\lambda_6^+}{\partial t}\right]\mathrm{H}(t - t_6). \tag{A.8}$$

Appendix B

The existence condition of a surface wave propagating along the piezoelectric–elastic bi-material interface is analyzed in this appendix. Substitution of (55)–(57) into (A.1) yields the reflected wave subjected to a dynamic anti-plane concentrated force as follows

$$\frac{p}{2\pi}\mathrm{Im}\left[\frac{R_4}{R_3}\frac{\partial\lambda_1^+}{\partial t}\right]\mathrm{H}(t - t_{1HD}), \tag{B.1}$$

where

$$R_3 = -(e_{15}^{(1)})^2\beta(\lambda_1^+) + \bar{c}_{44}^{(1)}\varepsilon_{11}^{(1)}\alpha(\lambda_1^+) + \mu\varepsilon_{11}^{(1)}\alpha^*(\lambda_1^+), R_4 = (e_{15}^{(1)})^2\beta(\lambda_1^+) + \bar{c}_{44}^{(1)}\varepsilon_{11}^{(1)}\alpha(\lambda_1^+) - \mu\varepsilon_{11}^{(1)}\alpha^*(\lambda_1^+),$$

$$b_2' = \sqrt{\frac{\rho^{(2)}}{\mu}}, \quad \alpha^*(\lambda_1^+) = \sqrt{b_2'^2 - (\lambda_1^+)^2}.$$

Considering the denominator of (B.1), let

$$R_3 = -(e_{15}^{(1)})^2\beta(\lambda_1^+) + \bar{c}_{44}^{(1)}\varepsilon_{11}^{(1)}\alpha(\lambda_1^+) + \mu\varepsilon_{11}^{(1)}\alpha^*(\lambda_1^+) = 0. \tag{B.2}$$

The principle of argument in Section III is applied to (B.2) and rewrite (B.2) in the form

$$R'(\lambda) = -(e_{15}^{(1)})^2\sqrt{\varepsilon^2 - \lambda^2} + \bar{c}_{44}^{(1)}\varepsilon_{11}^{(1)}\sqrt{b_1^2 - \lambda^2} + \mu\varepsilon_{11}^{(1)}\sqrt{b_2'^2 - \lambda^2} = 0. \tag{B.3}$$

Two cases, i.e., $b_1 > b_2'$ and $b_2' > b_1$, are discussed as follows Case (I): $b_1 > b_2'$. We find that if the condition

$$-(e_{15}^{(1)})^2\sqrt{b_1^2 - \varepsilon^2} + \mu\varepsilon_{11}^{(1)}\sqrt{b_1^2 - b_2'^2} > 0 \tag{B.4}$$

is satisfied, then the contours Γ_t', Γ_r' and Γ_l' in the v-plane is the same as that indicated in Fig. 4(a). The number of zeros for the function $R'(\lambda)$ is zero, i.e., $Z_\lambda = 2 \times \frac{1}{2} - 2 \times \frac{1}{2} = 0$. For the condition

$$-(e_{15}^{(1)})^2\sqrt{b_1^2 - \varepsilon^2} + \mu\varepsilon_{11}^{(1)}\sqrt{b_1^2 - b_2'^2} < 0, \tag{B.5}$$

the contours Γ_t', Γ_r' and Γ_1' in the v-plane is indicated in Fig. 4(b) and the number of zeros for the function $R'(\lambda)$ is two, i.e. $Z_\lambda = 2\times\frac{1}{2} + 2\times\frac{1}{2} = 2$. Case (II): $b_2' > b_1$. We find that

$$-(e_{15}^{(1)})^2\sqrt{b_2'^2-\varepsilon^2} + \bar{c}_{44}^{(1)}\varepsilon_{11}^{(1)}\sqrt{b_2'^2-b_1^2} > 0, \quad Z_\lambda = 0, \tag{B.6}$$

and

$$-(e_{15}^{(1)})^2\sqrt{b_2'^2-\varepsilon^2} + \bar{c}_{44}^{(1)}\varepsilon_{11}^{(1)}\sqrt{b_2'^2-b_1^2} < 0, \quad Z_\lambda = 2. \tag{B.7}$$

We have shown that the constraint of (B.5) (or (B.7)) is the existence condition of the surface wave. The surface wave velocity can be explicitly expressed as

$$v_s = \sqrt{\frac{2A_4}{-B_4 - \sqrt{B_4^2 - 4A_4C_4}}}, \tag{B.8}$$

where

$$\begin{aligned}
A_4 &= (1+\eta^2-k_e^4)^2 - 4\eta^2,\\
B_4 &= -2(b_1^2+\eta^2 b_2^2)(1+\eta^2-k_e^4) + 4\eta^2(b_1^2+b_2^2),\\
C_4 &= b_1^4 - 2\eta^2 b_1^2 b_2^2 + \eta^4 b_2^4,\\
\eta &= \frac{\mu}{\bar{c}_{44}^{(1)}}.
\end{aligned}$$

Appendix C. The static solutions for piezoelectric bi-materials

C.1. The static solutions for applying an anti-plane concentrated force

As indicated in Fig. 1, the material (1) is subjected to a static anti-plane concentrated force with magnitude p applied at $x = 0$ and $y = d$. The governing equations for the static problem are

$$\nabla^2 w = 0, \tag{C.1}$$

$$\nabla^2 \Phi = 0. \tag{C.2}$$

The constitutive equations are the same as that expressed in (13)–(16). The jump condition is

$$\tau_{yz}^{(1^+)}|_{y=d} - \tau_{yz}^{(1^-)}|_{y=d} = p\delta(x). \tag{C.3}$$

The continuous conditions are presented in (25)–(31). This problem can be solved by the application of the Fourier transform. The Fourier transform on the spatial variable x for (C.1) and (C.2) can be represented of the form

$$\frac{d^2\tilde{w}}{dy^2} - \omega^2\tilde{w} = 0, \tag{C.4}$$

$$\frac{d^2\tilde{\Phi}}{dy^2} - \omega^2\tilde{\Phi} = 0, \tag{C.5}$$

where ω is the Fourier transform parameter and the overwave symbol is used to denote the transform on the spatial variable x. The general solutions of (C.4) and (C.5) are

$$\begin{bmatrix}\tilde{w}^{(1^+)}\\ \tilde{\Phi}^{(1^+)}\end{bmatrix} = e^{\omega y}\begin{bmatrix}A_3\\ C_3\end{bmatrix} + e^{-\omega y}\begin{bmatrix}B_3\\ D_3\end{bmatrix}, \tag{C.6}$$

$$\begin{bmatrix} \tilde{w}^{(1^-)} \\ \tilde{\Phi}^{(1^-)} \end{bmatrix} = e^{\omega y} \begin{bmatrix} E_3 \\ G_3 \end{bmatrix} + e^{-\omega y} \begin{bmatrix} F_3 \\ H_3 \end{bmatrix}, \tag{C.7}$$

$$\begin{bmatrix} \tilde{w}^{(2)} \\ \tilde{\Phi}^{(2)} \end{bmatrix} = e^{\omega y} \begin{bmatrix} I_3 \\ K_3 \end{bmatrix} + e^{-\omega y} \begin{bmatrix} J_3 \\ L_3 \end{bmatrix}, \tag{C.8}$$

The static solutions in the transform domain are

$$\begin{bmatrix} \tilde{w}^{(1)} \\ \tilde{\Phi}^{(1)} \end{bmatrix} = \frac{-1}{2\omega^2} (e^{-\omega|y-d|}\mathbf{I} + e^{-\omega(y+d)}\hat{\mathbf{R}})\hat{\mathbf{M}}^{-1}\mathbf{Z}, \tag{C.9}$$

$$\begin{bmatrix} \tilde{w}^{(2)} \\ \tilde{\Phi}^{(2)} \end{bmatrix} = \frac{-1}{2\omega^2} e^{\omega(y-d)}\hat{\mathbf{T}}\hat{\mathbf{M}}^{-1}\mathbf{Z}, \tag{C.10}$$

where

$$\hat{\mathbf{R}} = (\hat{\mathbf{M}} + \hat{\mathbf{N}})^{-1}(\hat{\mathbf{M}} - \hat{\mathbf{N}}), \quad \hat{\mathbf{T}} = (\hat{\mathbf{M}} + \hat{\mathbf{N}})^{-1}(\hat{\mathbf{M}} - \hat{\mathbf{N}}) + \mathbf{I}, \quad \hat{\mathbf{M}} = \begin{bmatrix} c_{44}^{(1)} & e_{15}^{(1)} \\ e_{15}^{(1)} & -\varepsilon_{11}^{(1)} \end{bmatrix}, \quad \hat{\mathbf{N}} = \begin{bmatrix} c_{44}^{(2)} & e_{15}^{(2)} \\ e_{15}^{(2)} & -\varepsilon_{11}^{(2)} \end{bmatrix}.$$

After the Fourier inversion transform is employed, the static solutions for displacement, shear stresses and electric displacements are

$$\begin{bmatrix} w^{s(1)} \\ \Phi^{s(1)} \end{bmatrix} = \frac{1}{2\pi} (\hat{\mathbf{R}}\hat{\mathbf{M}}^{-1}\mathbf{Z}\ln r_1 + \hat{\mathbf{M}}^{-1}\mathbf{Z}\ln r_2), \tag{C.11}$$

$$\begin{bmatrix} w^{s(2)} \\ \Phi^{s(2)} \end{bmatrix} = \frac{1}{2\pi} \hat{\mathbf{T}}\hat{\mathbf{M}}^{-1}\mathbf{Z}\ln r_2, \tag{C.12}$$

$$\begin{bmatrix} \tau_{yz}^{s(1)} \\ D_y^{s(1)} \end{bmatrix} = \frac{1}{2\pi} \left(\hat{\mathbf{M}}\hat{\mathbf{R}}\hat{\mathbf{M}}^{-1}\mathbf{Z}\frac{y+d}{r_1^2} + \mathbf{Z}\frac{y-d}{r_2^2} \right), \tag{C.13}$$

$$\begin{bmatrix} \tau_{xz}^{s(1)} \\ D_x^{s(1)} \end{bmatrix} = \frac{1}{2\pi} \left(\hat{\mathbf{M}}\hat{\mathbf{R}}\hat{\mathbf{M}}^{-1}\mathbf{Z}\frac{x}{r_1^2} + \mathbf{Z}\frac{x}{r_2^2} \right), \tag{C.14}$$

$$\begin{bmatrix} \tau_{yz}^{s(2)} \\ D_y^{s(2)} \end{bmatrix} = \frac{1}{2\pi} \hat{\mathbf{N}}\hat{\mathbf{T}}\hat{\mathbf{M}}^{-1}\mathbf{Z}\frac{y-d}{r_2^2}, \tag{C.15}$$

$$\begin{bmatrix} \tau_{xz}^{s(2)} \\ D_x^{s(2)} \end{bmatrix} = \frac{1}{2\pi} \hat{\mathbf{N}}\hat{\mathbf{T}}\hat{\mathbf{M}}^{-1}\mathbf{Z}\frac{x}{r_2^2}. \tag{C.16}$$

C.2. The static solutions for applying an electric charge

The jump condition is

$$D_y^{(1^+)}|_{y=d} - D_y^{(1^-)}|_{y=d} = -q\delta(x). \tag{C.17}$$

The static solutions for displacement, shear stresses and electric displacements in piezoelectric materials (1) and (2) are presented as follows

$$\begin{bmatrix} w^{s(1)} \\ \Phi^{s(1)} \end{bmatrix} = \frac{1}{2\pi} (\hat{\mathbf{R}}\hat{\mathbf{M}}^{-1}\mathbf{G}\ln r_1 + \hat{\mathbf{M}}^{-1}\mathbf{G}\ln r_2), \tag{C.18}$$

$$\begin{bmatrix} w^{s(2)} \\ \Phi^{s(2)} \end{bmatrix} = \frac{1}{2\pi}\hat{\mathbf{T}}\hat{\mathbf{M}}^{-1}\mathbf{G}\ln r_2, \tag{C.19}$$

$$\begin{bmatrix} \tau_{yz}^{s(1)} \\ D_y^{s(1)} \end{bmatrix} = \frac{1}{2\pi}\left(\hat{\mathbf{M}}\hat{\mathbf{R}}\hat{\mathbf{M}}^{-1}\mathbf{G}\frac{y+d}{r_1^2} + \mathbf{G}\frac{y-d}{r_2^2}\right), \tag{C.20}$$

$$\begin{bmatrix} \tau_{xz}^{s(1)} \\ D_x^{s(1)} \end{bmatrix} = \frac{1}{2\pi}\left(\hat{\mathbf{M}}\hat{\mathbf{R}}\hat{\mathbf{M}}^{-1}\mathbf{G}\frac{x}{r_1^2} + \mathbf{G}\frac{x}{r_2^2}\right), \tag{C.21}$$

$$\begin{bmatrix} \tau_{yz}^{s(2)} \\ D_y^{s(2)} \end{bmatrix} = \frac{1}{2\pi}\hat{\mathbf{N}}\hat{\mathbf{T}}\hat{\mathbf{M}}^{-1}\mathbf{G}\frac{y-d}{r_2^2}, \tag{C.22}$$

$$\begin{bmatrix} \tau_{xz}^{s(2)} \\ D_x^{s(2)} \end{bmatrix} = \frac{1}{2\pi}\hat{\mathbf{N}}\hat{\mathbf{T}}\hat{\mathbf{M}}^{-1}\mathbf{G}\frac{x}{r_2^2}. \tag{C.23}$$

References

Achenbach, J.D., 1976. Wave Propagation in Elastic Solids. Elsevier, New York.

Bleustein, J.L., 1968. A new surface wave in piezoelectric materials. Appl. Phys. Lett. 13, 412–413.

Cagnard, L., 1962. Reflection and Refraction of Progressive Waves. McGraw-Hill, New York.

Camou, S., Laude, V., 2003. Interface acoustic waves properties in some common crystal cuts. IEEE Trans. Ultrason. Ferroelec. Freq. Contr. 50, 1363–1370.

de Hoop, A.T., 1960. A modification of Cagniard's method for solving seismic pulse problems. Appl. Sci. Res. 8, 349–356.

Dvoesherstov, M.Y., Cherednik, V.I., Chirimanov, A.P., Petrov, S.G., 2002. Properties of acoustic boundary waves propagating along the interface between two piezoelectric media. Acoust. Phys. 48, 766–769.

Gulayev, Y.V., 1969. Electroacoustic surface waves in solids. Sov. Phys. JETP 9, 37–38.

Hayt, W.H., Buck, J.A., 2001. Engineering Electromagnetics. Mc Graw Hill, New York.

Honein, B., Herrman, G., 1992. Wave propagation in non-homogeneous piezoelectric materials. Act. Contr. Noise Vib. 38, 105–112.

Irino, T., Shirosaki, Y., Shimizu, Y., 1988. Propagation of boundary acoustic waves along a ZnO layer between two materials. IEEE Trans. Ultrason. Ferroelec. Freq. Contr. 33, 701–707.

Irino, T., Shimizu, Y., 1989. Optimized Stoneley wave device by proper choice of glass overcoat. IEEE Trans. Ultrason. Ferroelec. Freq. Contr. 36, 159–167.

Lamb, H., 1904. On the propagation of tremors over the surface of an elastic solid. Philos. Trans. R. Soc. A 203, 1–42.

Li, S., 1996. The electromagneto-acoustic surface wave in a piezoelectric medium: The Bleustein-Gulyaev mode. J. Appl. Phys. 80, 5264–5269.

Ma, C.C., Huang, K.C., 1993. Exact transient solutions of buried dynamic point forces for elastic bi-materials. Int. J. Solids Struct. 33, 4511–4529.

Maerfeld, C., Tournois, P., 1971. Pure shear elastic surface wave guided by the interface of two semi-infinite media. Appl. Phys. Lett. 19, 117–125.

Pao Y.H., Gajewski, R., 1977. The generalized ray theory and transient responses of layered elastic solids. In: Phys. Acoust., vol. 13, Academic, New York, pp. 184–266.

Royer, D., Dieulesaint, E., 2000. Elastic Wave in Solid I. Springer, Berlin, Heidelberg, Germany.

Spencer, T.W., 1960. The method of generalized reflection and transmission coefficients. Geophys. J. 25, 625–641.

Stoneley, R., 1924. Elastic waves at the surface of separation of two solids. Proc. R. Soc. Lond. A 106, 416–428.

Tseng, C.C., 1970. Piezoelectric surface waves in cubic crystals. J. Appl. Phys. 41, 2270–2276.

Yamanouchi, M., 1990. Proceedings of the First International Symposium on Functionally Gradient Materials. Sendai, Japan.

Yamashita, T., Hashimito, K., Yamaguchi, M., 1997. Highly piezoelectric shear-horrizontal-type boundary waves. Jpn. J. Appl. Phys. 36, 3057–3059.